Response of the Wintertime Northern Hemisphere Atmospheric Circulation to Current and Projected Arctic Sea Ice Decline: A Numerical Study with CAM5

YANNICK PEINGS AND GUDRUN MAGNUSDOTTIR

Department of Earth System Science, University of California, Irvine, Irvine, California

(Manuscript received 17 May 2013, in final form 26 August 2013)

ABSTRACT

The wintertime Northern Hemisphere (NH) atmospheric circulation response to current (2007–12) and projected (2080–99) Arctic sea ice decline is examined with the latest version of the Community Atmospheric Model (CAM5). The numerical experiments suggest that the current sea ice conditions force a remote atmospheric response in late winter that favors cold land surface temperatures over midlatitudes, as has been observed in recent years. Anomalous Rossby waves forced by the sea ice anomalies penetrate into the stratosphere in February and weaken the stratospheric polar vortex, resulting in negative anomalies of the northern annular mode (NAM) that propagate downward during the following weeks, especially over the North Pacific. The seasonality of the response is attributed to timing of the phasing between the forced and climatological waves. When sea ice concentration taken from projections of conditions at the end of the twenty-first century is prescribed to the model, negative anomalies of the NAM are visible in the troposphere, both in early and late winter. This response is mainly driven by the large warming of the lower troposphere over the Arctic, as little impact is found in the stratosphere in this experiment. As a result of the thermal expansion of the polar troposphere, the westerly flow is decelerated and a weak but statistically significant increase of the midlatitude meanders is identified. However, the thermodynamical response extends beyond the Arctic and offsets the dynamical effect, such that the stronger sea ice forcing has limited impact on the intensity of cold extremes over midlatitudes.

1. Introduction

The observed decrease of the Arctic sea ice is one of the most obvious signs of the current global climate change and has been larger than the projections of the Intergovernmental Panel on Climate Change (Solomon et al. 2007) for the past few years (Stroeve et al. 2007, 2012). Owing to cryospheric feedback processes, the observed surface warming is greater over the Arctic than in other regions of the globe (Serreze and Francis 2006; Screen and Simmonds 2010). This so-called Arctic amplification effect is associated with a strong decrease of the sea ice extent, especially during summer and fall (Serreze et al. 2007; Stroeve et al. 2011). This signal has been particular strong in recent years, with exceptionally low sea ice extent at the end of summer (Comiso et al. 2008). The sea ice volume is also declining (Kurtz et al. 2011), enhancing the sea ice–albedo feedback (a thinner ice recovers less readily) and increasing the odds of a sea-ice-free Arctic in the coming decades (Overland and Wang 2013). In addition to the increased surface temperature, atmospheric synoptic variability in the form of wind forcing has also played a role in the recent collapse of the Arctic sea ice (Ogi and Wallace 2012; Overland et al. 2012; Simmonds and Rudeva 2012).

Sea ice is an important part of the climate system. It exerts a strong influence on the surface energy budget by modulating the surface heat fluxes from the ocean as well as the surface albedo. A decline of the Arctic sea ice can significantly impact other components of the climate system, including the Northern Hemisphere (NH) atmospheric circulation. Given the intrinsic variability of the atmosphere and the numerous external factors that influence it, modeling studies are useful for isolating the contributions of each forcing. The influence of sea ice anomalies on the atmosphere has been extensively studied using atmospheric general circulation models (AGCMs) (see review in Budikova 2009). Some studies (Magnusdottir et al. 2004; Deser et al. 2004, 2007) have

Corresponding author address: Yannick Peings, Dept. of Earth System Science, University of California, Irvine, 3200 Croul Hall, Irvine, CA 92697-3100.
E-mail: ypeings@uci.edu

DOI: 10.1175/JCLI-D-13-00272.1

examined the effect of exaggerated sea ice anomalies over the North Atlantic region that correspond to sea ice anomalies forced by the North Atlantic Oscillation (NAO) (Deser et al. 2000), the primary mode of wintertime atmospheric variability in the region. These studies revealed a negative feedback from the sea ice anomalies onto the NAO or its hemispheric expression, the northern annular mode (NAM) (Thompson and Wallace 2000). This negative feedback has also been identified in the observational record (Strong et al. 2009). North Pacific sea ice anomalies force a stationary wave train that propagates downstream across the Pacific basin (Honda et al. 1999) and can modulate the intensity/position of the Siberian high, Aleutian low, and the west Pacific pattern (Liu et al. 2007; Linkin and Nigam 2008; Matthewman and Magnusdottir 2011). Other studies have investigated the effect of the overall Arctic sea ice extent and/or concentration anomalies on the NH atmospheric circulation, using observed sea ice anomalies (Alexander et al. 2004; Bhatt et al. 2008; Balmaseda et al. 2010; Kumar et al. 2010; Strey et al. 2010; Blüthgen et al. 2012; Orsolini et al. 2012; Porter et al. 2012; Cassano et al. 2013), projected anomalies for the end of the twenty-first century (Singarayer et al. 2006; Seierstad and Bader 2009; Deser et al. 2010), or a sea ice free ocean prescribed in summer and over the entire year (Semmler et al. 2012). Owing to the diversity of the forcings/models used, these studies report a wide range of local and remote atmospheric responses. Generally, the signal-to-noise ratio of the remote response is low, and a large number of ensemble members is necessary to detect a significant signal (Screen et al. 2013a). The early winter transient response is rather baroclinic and tends to become equivalent barotropic during the midlate winter (Magnusdottir et al. 2004; Deser et al. 2007, 2010). It sometimes projects onto the NAO–NAM mode, with different amplitudes and timings dependent on the study (Alexander et al. 2004; Seierstad and Bader 2009; Deser et al. 2010). Moreover, significant impacts have been reported at the synoptic scale, especially on storm track activity over the North Atlantic in late winter (Magnusdottir et al. 2004; Seierstad and Bader 2009). To assess the effect of the recent increasing rate of sea ice decline, Screen et al. (2013b) prescribed the observed trend of Arctic sea ice concentration in experiments performed with two different AGCMs. Except for a slight negative NAO-like response in early winter, they did not identify a significant NH atmospheric circulation response.

Several studies suggest that the recent Arctic amplification can increase the likelihood of extreme events over the midlatitudes, such as cold spells or extensive snowfall (Honda et al. 2009; Francis et al. 2009; Petoukhov and Semenov 2010; Liu et al. 2012; Tang et al. 2013). Furthermore, some authors believe that the recent sea ice decline is involved in the recent negative trend of the NAO–NAM (Cohen et al. 2012). These ideas have gained support by the cold winters and extreme events observed during recent years over Europe, North America, and Asia (Cattiaux et al. 2010; Coumou and Rahmstorf 2012). Because of the warming of the Arctic troposphere, the poleward gradient of the tropospheric thickness has decreased over recent years and weakened the westerly flow, in line with thermal wind arguments (Francis and Vavrus 2012). According to the latter study, the meridional amplitude of midlatitude planetary waves has increased and the eastward propagation of Rossby waves in the upper-level flow has slowed down, which they interpret as favoring the persistence of extreme events. If confirmed, this result would reconcile the occurrence of cold extremes over midlatitudes with the observed global warming. However, any significant change in wave amplitude is hard to detect in atmospheric reanalyses (Screen and Simmonds 2013), and this issue deserves additional investigations using numerical experiments to isolate the contribution of sea ice from those of other processes.

The effect of Arctic amplification on the recent tendency toward a negative NAO/NAM and more numerous extreme events in winter is difficult to discern from observations due to the short observational record of Arctic sea ice concentrations and the high natural variability of the high-latitude atmospheric circulation. Moreover, the atmospheric response to a projected continuous decline of sea ice in the future is uncertain, especially whether the response will project onto the NAM (Cattiaux and Cassou 2013). In this study, we revisit the impact of the Arctic sea ice decline on the NH atmospheric circulation using the latest version of the Community Atmospheric Model, CAM5, from the National Center for Atmospheric Research (NCAR). We examine the large-scale response of the NH atmosphere by imposing in the model two different sea ice forcings representative of the recent and projected sea ice decline over the Arctic. Our two sensitivity experiments are forced with sea ice concentration of the 2007–12 period obtained from observations and a sea ice concentration taken from coupled climate simulations of the end of the twenty-first century. The physical mechanisms are examined in detail in order to explain the timing and sensitivity of the response to the sea ice forcing. The effect of sea ice loss on the meridional wave amplitude and on cold extreme temperatures over midlatitudes is also investigated.

The paper outline is as follows. Section 2 describes the experiments and the methodology used to prescribe the sea ice perturbation in our model. Section 3 presents the wintertime response of the atmosphere in both

experiments and discusses the physical mechanisms at work in the model. A subsection is dedicated to the response of extreme events over the midlatitudes. Finally, section 4 contains a discussion and some concluding remarks.

2. Model and experiments

The atmospheric model used in this study is CAM5, which is the latest version of CAM at the time of the study and includes a new physics scheme as well as a better representation of aerosols. The major improvements in this version concern cloud properties, including a more realistic seasonal cycle of Arctic clouds (Kay et al. 2012b). CAM5 is the atmospheric component of the Community Earth System Model (CESM) (Neale et al. 2011) and is coupled to the Community Land Model (CLM). The resolution used in this study is 1.9° latitude and 2.5° longitude with 30 vertical levels. The control experiment (CTL) is a 50-yr simulation with a prescribed annually repeating sea surface temperature (SST) and sea ice concentration (SIC, in % of the domain covered by ice) that represents climatology for the 1979–2000 period. The climatological annual cycle prescribed to the model comes from the monthly Hadley Centre Sea Ice and Sea Surface Temperature (HadISST) dataset (Rayner et al. 2003). It is a 1°-resolution product in which sea ice is retrieved from various sources of digitized sea ice charts and passive microwave imagery. One year of spinup is conducted before extracting the output from the simulations. Greenhouse gas and aerosol concentrations are representative of present-day conditions (year 2000). Two perturbation experiments, each consisting of 50-member ensembles, are paired to this control run such that they only differ by the SIC/SST boundary conditions. Each ensemble member is started from initial conditions in CTL corresponding to 1 April and is run for 13 months so that it spans an entire annual cycle (May to April, the first month is removed owing to spinup).

- The first perturbation experiment (2010C, for observed sea ice concentration of 2007–12) was designed to assess the impact of recent SIC conditions over the Arctic on the NH atmospheric circulation. The monthly SIC annual cycle prescribed to the model over the Arctic is computed from the 2007–12 period of the HadISST dataset. SSTs are set to the 1979–2000 climatology except for regions where sea ice has substantially changed in order to include the SST warming effect owing to sea ice loss (Screen et al. 2013b). For each month, if the 2007–12 SIC climatology differs by 10% or more from its 1979–2000 value in the Northern Hemisphere, the SST is changed to the 2007–12 climatological value of the corresponding month. Otherwise, SST is set to the 1979–2000 climatological value. Thus, only changes in Arctic sea ice and the SST changes directly associated with sea ice changes are taken into account.
- The design of the second perturbation experiment (2090C, for 2090 sea ice concentration) is the same except the sea ice forcing is stronger. This forcing comes from simulations performed for phase 5 of the Coupled Model Intercomparison Project (CMIP5) with the Community Climate System Model, version 4 (CCSM4), which is the previous version of the coupled ocean–atmosphere model from CESM. The 2080–99 climatological annual cycle of SIC is taken from the 6-member ensemble mean of the twenty-first-century simulations performed under the $8.5\,W\,m^{-2}$ representative concentration pathway (RCP85) scenario. The SST change is taken into account in the same way as for 2010C, only over high-latitude areas where SIC has substantially changed. The 2080–99 ensemble-average SST from the coupled simulations is used over these regions, while SST is set to the 1979–2000 climatology elsewhere. As 2090C is compared to CTL, simulated and observed sea ice concentrations are compared. Consequently, the 2090C–CTL anomalies do not only include the effect of anthropogenic forcings, but also anomalies due to the model biases in the representation of the sea ice concentration. However, we found that this effect is negligible. Subtracting the 2090C sea ice concentration from the ensemble-mean SIC from six historical CCSM4 runs (over the same 1979–2000 period) results in SIC anomalies that are very similar to the 2090C–CTL SIC anomalies (not shown).

Note that the ice thickness is not modified in these experiments and is fixed to 2 m throughout the Arctic. The ensemble mean of each experiment is computed by averaging the 50 members, and the climate response is found for certain climate variables by subtracting the 50-yr average for that variable in CTL from the ensemble mean of the variable in 2010C and 2090C. A two-sided Student's t test is used to compare the ensemble means from different experiments and assess the statistical significance of the response. The remote response to the sea ice forcing is low compared to the NH internal atmospheric variability (e.g., Screen et al. 2013a), such that a large ensemble of members is needed to obtain a significant signal. In our case, an ensemble of 50 members is sufficient to detect a robust response in the NH atmospheric circulation.

The SIC/SST prescribed to the model for each experiment are depicted in Figs. 1 and 2. Figure 1a shows the annual cycle of SIC (left axis, solid lines) and SST (right

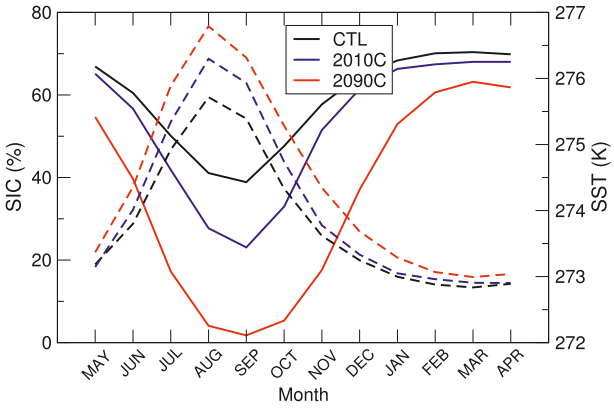

FIG. 1. Annual cycles of SIC (solid lines, left ordinate) and SST (dashed lines, right ordinate) averaged over the Arctic Ocean (north of 60°N) for CTL, 2010C, and 2090C.

axis, dashed lines) averaged north of 60°N. The SIC is decreased over the entire year in the two perturbation experiments, with a higher amplitude in late summer and autumn. The SIC forcing is greater in 2090C, the Arctic Ocean is almost free of sea ice in September in this experiment. The SST anomalies are of opposite sign with maximum positive anomalies in summer. The spatial distribution of the SIC/SST anomalies in winter [December to February (DJF)] is shown in Fig. 2. In the 2010C experiment, sea ice is decreased over the Barents, Kara, and Okhotsk Seas and is slightly increased near Bering Strait and in Baffin Bay (Fig. 2b). Note that the SIC/SST forcing not only includes the Arctic Ocean but also some midlatitude anomalies (especially in the Sea of Okhotsk). However, ice in these regions is part of the seasonal sea ice distribution and is therefore included in the definition of "Arctic" sea ice in this paper. In 2090C, the sea ice anomalies are always negative and are larger than in 2010C, both in amplitude and in spatial extent (Fig. 2c). They are associated with positive SST anomalies that can exceed 2.5 K in 2090C (Figs. 2e,f). Note that the 2010C forcing is close to the one used by Screen et al. (2013b) except that they use the 1979–2011 trend instead of the 2007–12 anomalies to force the model. The 2090C forcing is comparable with the one used by Deser et al.

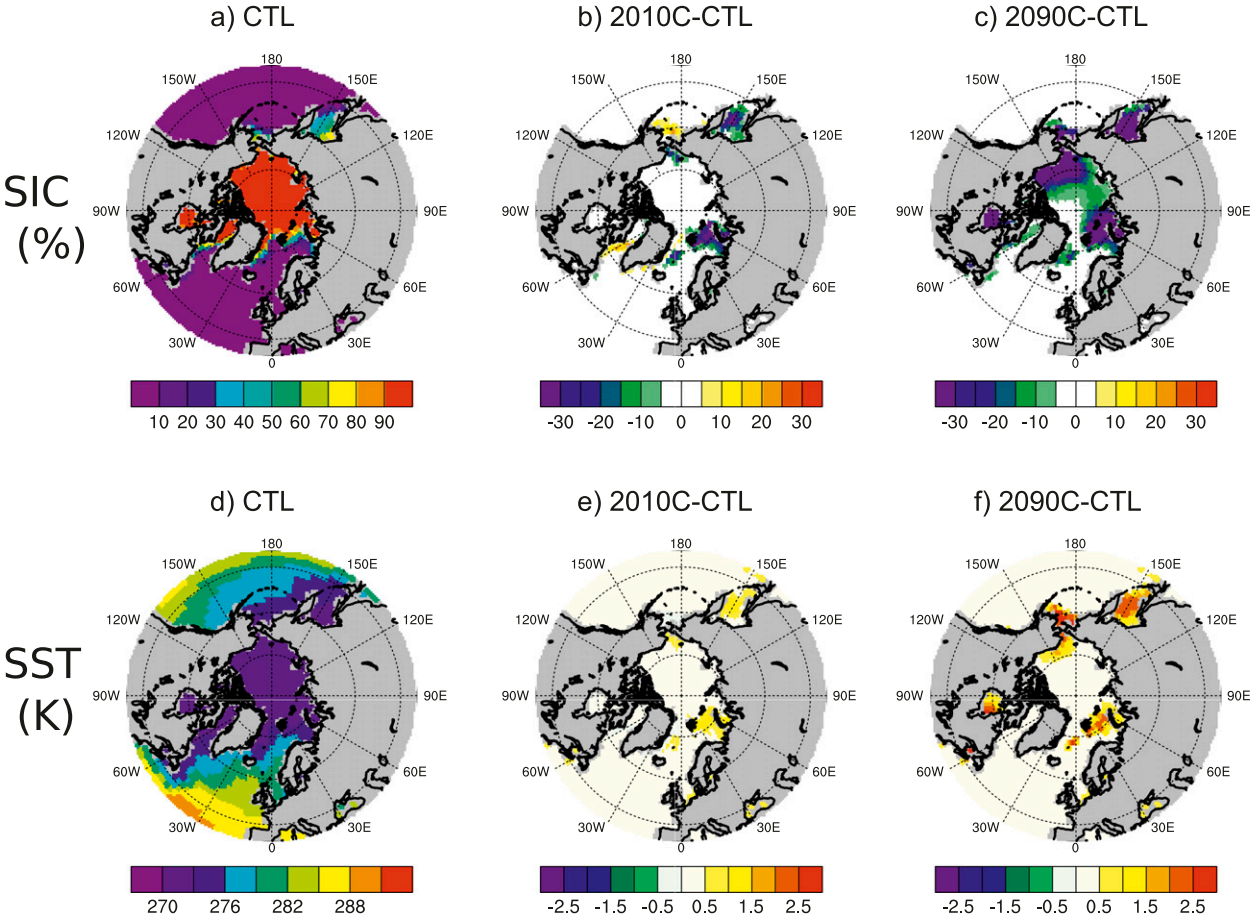

FIG. 2. Winter mean (DJF) of (a) SIC climatology in CTL (%) and SIC anomalies prescribed (b) in 2010C and (c) in 2090C; (d)–(f) as in (a)–(c) but for SST (K).

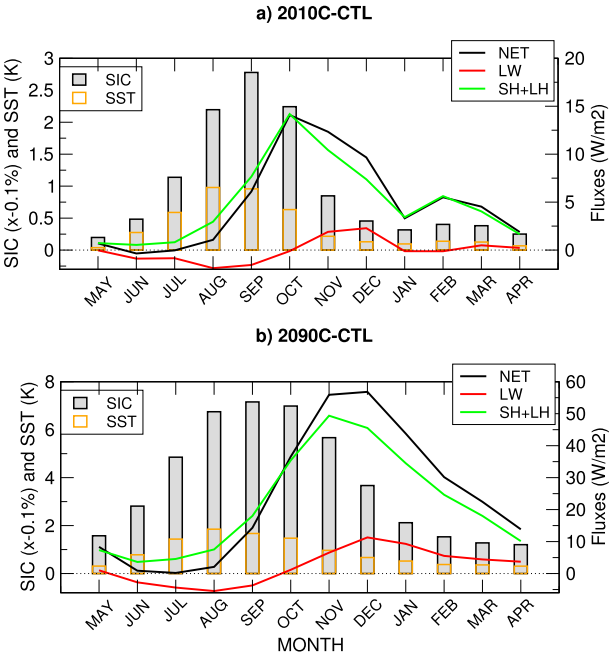

FIG. 3. (a) Month-to-month response for 2010C of the net surface energy released to the atmosphere (black curve), the longwave radiative flux (red curve), and the turbulent fluxes (sensible + latent heat fluxes, green curve) averaged over the sea-ice-covered region in CTL (SIC > 10%) north of 40°N: fluxes (W m^{-2}, scale on the right ordinate). The monthly SIC anomalies (gray bars, multiplied by −0.1 for display) and SST anomalies (orange bars) are indicated (scale on the left ordinate). (b) As in (a) but for 2090C.

(2010). However, these two studies were conducted with CAM3, which is an earlier version of the atmospheric GCM that we use (CAM5).

3. Results

We focus on the wintertime response in this study. First we examine the average atmospheric response over the entire winter season (DJF) and then investigate the mechanisms of the different responses obtained in each experiment. We conclude this section by examining the change in planetary wave amplitude and the occurrence of cold extreme events over midlatitudes.

a. Atmospheric response in winter

The sea ice cover strongly influences the surface turbulent heat fluxes, the radiative fluxes, and consequently the surface temperature. The effect of sea ice anomalies on the surface energy budget is depicted for each month of the two perturbation experiments in Fig. 3. The response of the net surface energy flux, net longwave radiation, and turbulent fluxes (sensible + latent) are shown, as well as the SIC and SST anomalies, averaged over the sea ice covered area in the Arctic and midlatitudes (north of 40°N). The average only includes pixels where sea ice is present in CTL (SIC > 10%). The net surface energy flux is computed as the sum of the net longwave radiation and of the turbulent fluxes. The shortwave radiation is not included because its changes do not impact the surface budget over the ocean (prescribed SST/SIC mode), but the ice–albedo feedback is implicitly included in the turbulent and longwave fluxes through the changes in SST where the sea ice concentration is modified. Positive values of the fluxes indicate an atmospheric gain in energy. The removal of SIC (and the associated warming of SST) increases the net surface energy flux from the end of summer until December (April) in 2010C (2090C). The main contribution is from the turbulent fluxes. The longwave radiation has a positive contribution in early winter in 2010C—through the entire winter in 2090C. Note that the vertical scale is not the same in Figs. 3a and 3b since the amplitude of the flux anomalies is much greater in 2090C (approximately four times greater). The response of the net surface energy flux lags the maximum in SIC/SST anomalies. The SIC/SST anomalies are maximum in summer, while the anomalies of the surface energy budget are maximum from September to December in 2010C (Fig. 3a)—and from September to February in 2090C (Fig. 3b). This lag was previously reported in modeling experiments and in reanalyses (Seierstad and Bader 2009; Deser et al. 2010; Screen et al. 2013b; Screen and Simmonds 2010). It is related to the enhancement of the turbulent fluxes during fall and winter when the lower atmosphere cools more rapidly than the ocean.

Figure 4 shows the spatial distribution of the response in net surface energy flux in both experiments and for each individual month in winter (December, January, and February). A positive response (gain in heat by the atmosphere) is found where the sea ice is removed and SSTs are warmer. A negative response is found over the small regions of positive SIC anomalies in 2010C (Bering Strait and Baffin Bay, Figs. 4a–c). Significant negative anomalies are also found south of the sea ice edge, especially in 2090C (Figs. 4d–f). This is due to the following reason: the atmospheric warming induced by the removal of sea ice spreads beyond the SIC/SST anomalies. As the atmosphere is warmer, the heat flux directed from the atmosphere to ocean is increased. In nature, the ocean would warm, reducing the air–sea contrast and the amplitude of these negative anomalies. In our case, the ocean is not interactive and SSTs are not modified in these regions where the SIC does not change, leading to exaggerated negative anomalies of the net surface energy flux. This behavior is commonly found in SIC-perturbation

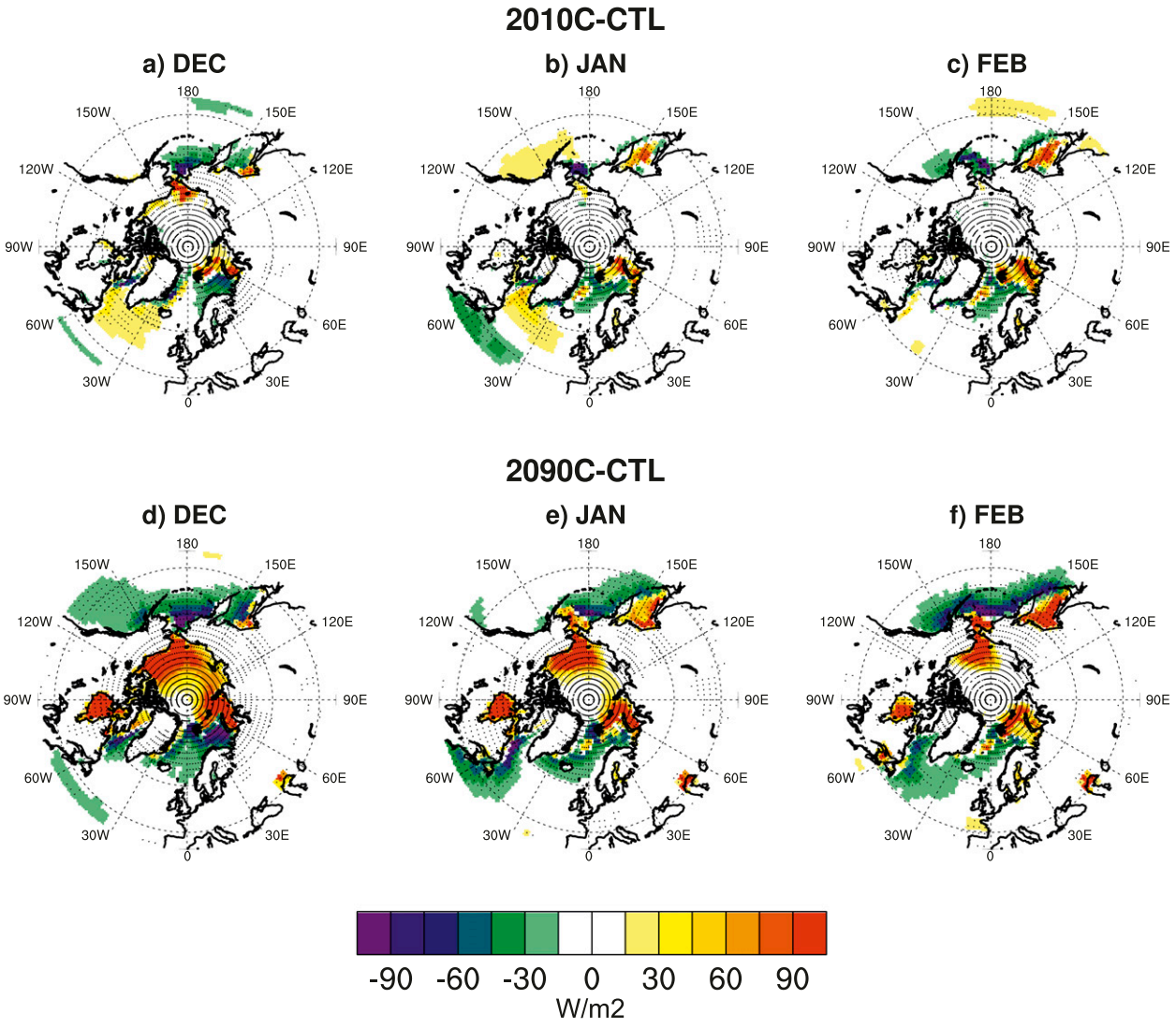

FIG. 4. Response of the net surface energy flux (turbulent fluxes + net longwave radiation, $W m^{-2}$) in 2010C for (a) December, (b) January, and (c) February. Positive (negative) values indicate a gain (loss) of energy by the atmosphere. Anomalies significant at the 95% confidence level are stippled. (d)–(f) As in (a)–(c) but for 2090C.

experiments with a noninteractive ocean (Deser et al. 2010; Screen et al. 2013b).

Figure 5 highlights the wintertime 2-m temperature response associated with these changes in the surface energy budget. Figure 5a shows the mean winter 2-m temperature averaged over the control simulation (CTL), Fig. 5b shows the temperature response in 2010C (2010C minus CTL), Fig. 5c the response in 2090C (2090C minus CTL), and Fig. 5d the difference between the two perturbation experiments (2090C minus 2010C). In 2010C (Fig. 5b), positive anomalies spread beyond the negative sea ice anomalies over the Arctic Ocean, and local negative anomalies are found where the SIC is increased (Fig. 2b). A moderate but significant cooling is found in midlatitudes over Asia but not over Europe and North America. The temperature response in 2090C is much greater, both in amplitude and in spatial extent (Figs. 5c,d; note the different scale in Fig. 5d). The average warming is ~8 K over the Arctic Ocean and spreads over the northern part of the continents, to 45°N over some sectors. The model does not simulate a significant cooling of the midlatitudes, except over limited areas of Eurasia. The midlatitude cooling is weaker than in 2010C (Fig. 5d), suggesting that there is not a linear relationship between a decrease of Arctic sea ice and lower temperatures over midlatitudes. A more complete discussion of this result is found in section 3d where the response in terms of extreme temperatures is investigated.

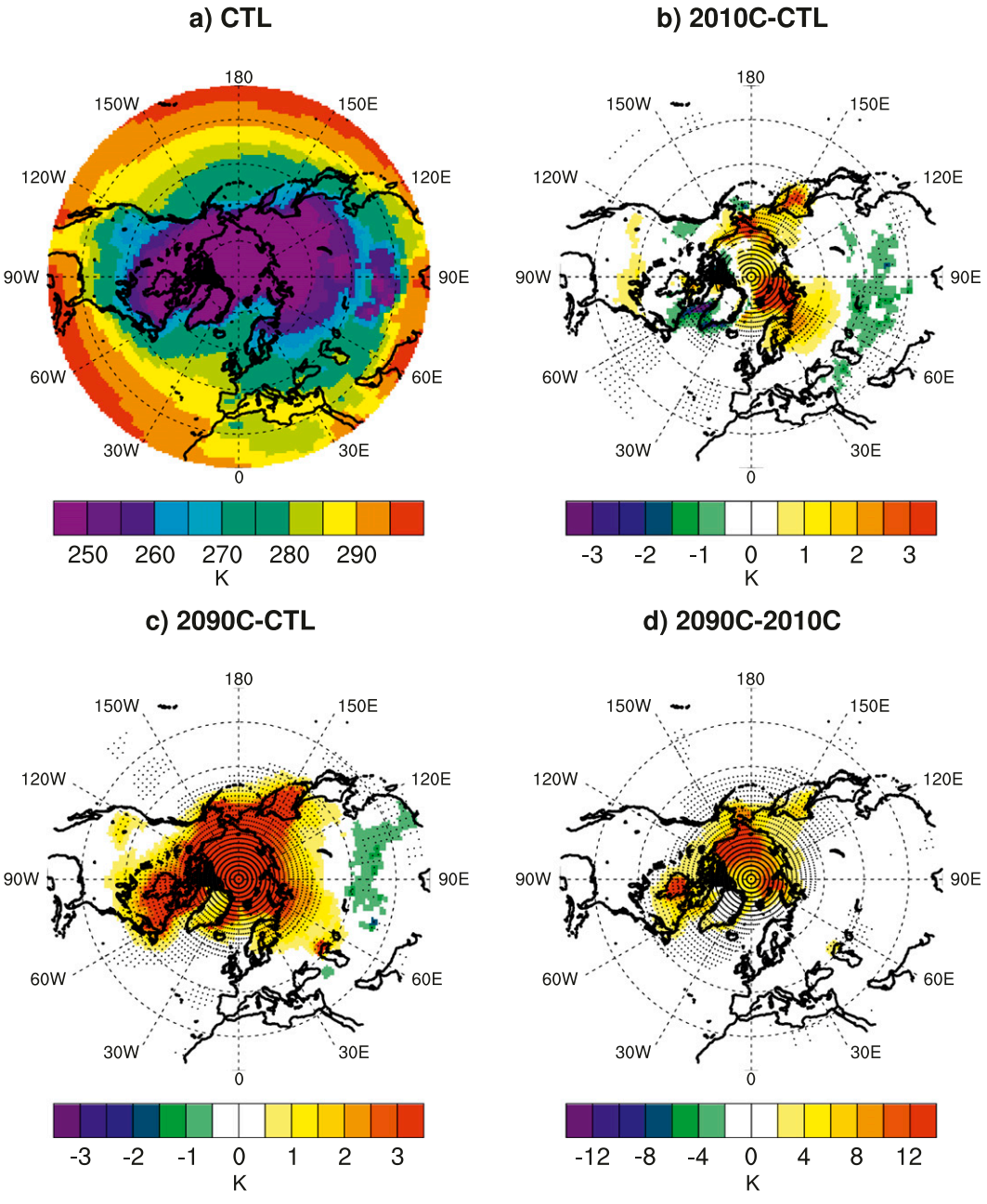

FIG. 5. (a) Mean winter (DJF) 2-m temperature climatology (K) for CTL. Response in 2-m temperature for (b) 2010C and (c) 2090C; (d) difference between (c) and (b) (2090C − 2010C). Anomalies significant at the 95% confidence level are stippled. Note the difference of scale in (d).

Figure 6 shows the mean winter NH (north of 20°N) atmospheric response in sea level pressure (SLP) and in midtropospheric geopotential (500-hPa geopotential: Z_{500}) for both experiments. In line with the results of Screen et al. (2013b), the current sea ice anomalies do not force a strong response of the mean wintertime atmospheric circulation in 2010C (Figs. 6b,e). Both for SLP and Z_{500}, the response is significant at the 95% confidence level only over limited regions in the NH. Nevertheless, the response depends on the month considered and it is highly significant in February over the North Pacific (not shown but this result is further discussed in section 3b). The results are more significant in 2090C, consistent with the stronger forcing imposed on the model in that experiment. The winter-mean response is baroclinic over the Arctic (low SLP anomalies associated with a ridge at

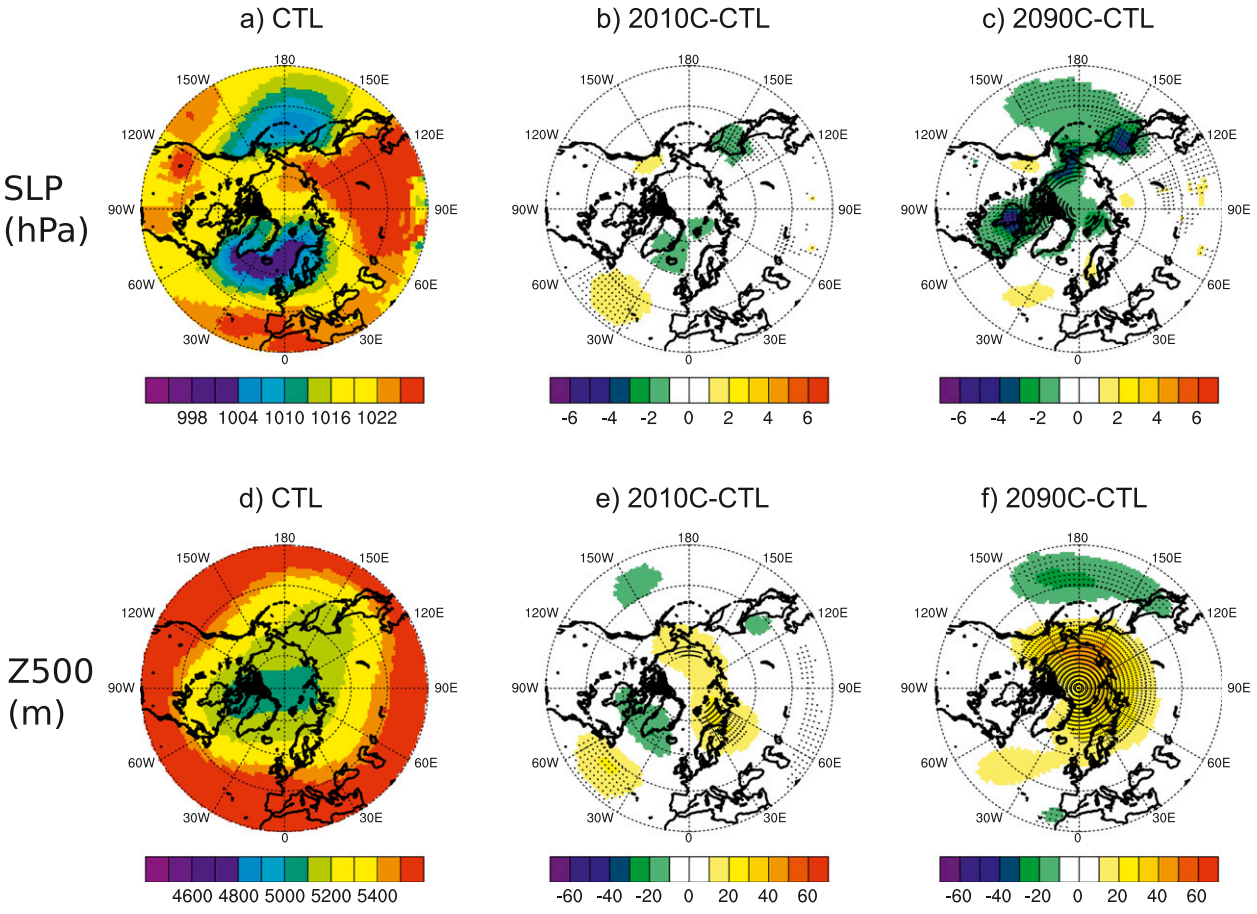

FIG. 6. (a) Mean winter (DJF) sea level pressure climatology (hPa) for CTL and the response in SLP (b) for 2010C and (c) for 2090C; (d)–(f) as in (a)–(c) but for the 500-hPa geopotential (m). Anomalies significant at the 95% confidence level are stippled.

500 hPa) and barotropic in midlatitudes, especially over the North Pacific (Figs. 6c,f). These results are consistent with those from Deser et al. (2010) that found a baroclinic response over the Arctic in early and midwinter. However, the barotropic negative anomaly over the North Pacific is larger in the present study. The Z_{500} response resembles the negative phase of the NAM, even though the anomalies over the North Atlantic basin are too small. The response is consistent with previous studies that identified such a response in late winter (Alexander et al. 2004; Seierstad and Bader 2009; Deser et al. 2010). It is maximum in February in our study, but is also visible in early winter as discussed in the next paragraph. This negative NAM signal is present in the free troposphere but does not project clearly onto the SLP (Fig. 6c) and other surface variables such as the 2-m temperature (Fig. 5c) or precipitation (not shown).

To examine the intraseasonal evolution of the geopotential response, the daily evolution of the vertical distribution of horizontally averaged geopotential over the polar cap (north of 65°N) is plotted in Fig. 7. This diagnostic is a good proxy for the daily evolution of the NAM index as a function of altitude (Baldwin and Thompson 2009), where a positive (negative) anomaly is associated with a negative (positive) value of the NAM index. In line with the results from Fig. 6, we do not find a significant response in 2010C for most of the winter (Fig. 7a). However, a significant positive anomaly is found at the end of winter from the beginning of February until the middle of March. This anomaly, which represents a weakening of the stratospheric polar vortex, emerges in the stratosphere in February and propagates toward the troposphere in the following weeks. It reaches the surface around mid-February and is associated with a strong tropospheric signal located at the surface over the North Pacific (see section 3b). This downward propagation of stratospheric anomalies is a well-known mechanism by which stratospheric sudden warmings (SSWs) impact the NH climate (Baldwin and Dunkerton 2001; Polvani and Waugh 2004). The response depicted in Fig. 7a is not strong enough to be classified as a SSW (no reversal of the westerly wind at 10 hPa, 60°N), but this

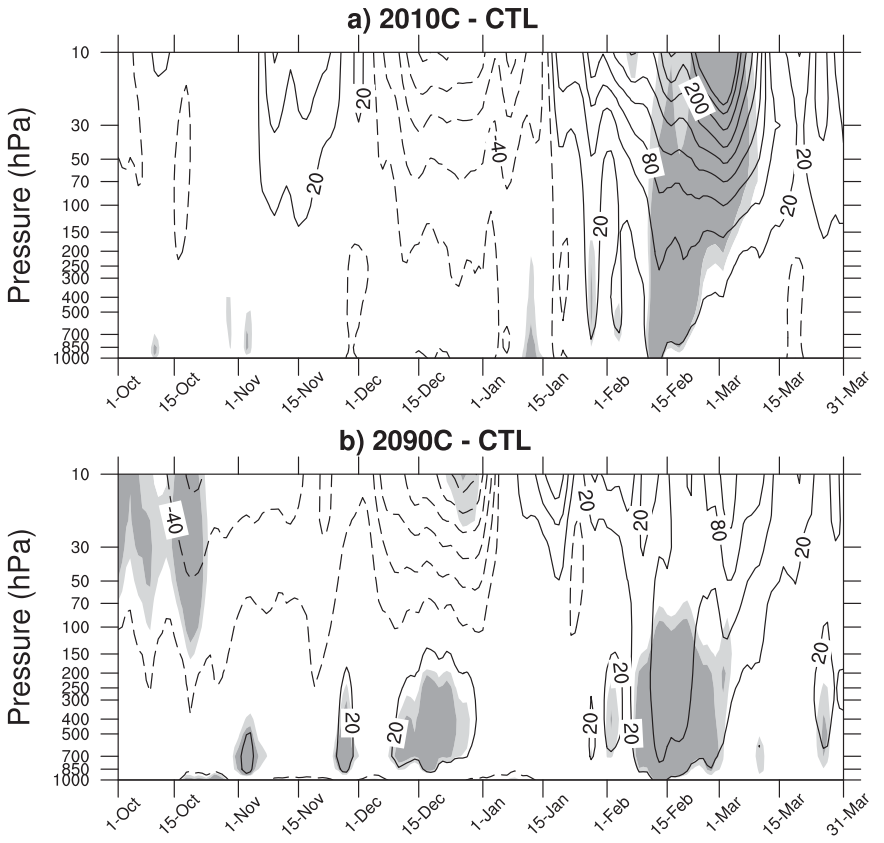

FIG. 7. Time–pressure cross section of the daily polar cap response in geopotential (m) averaged north of 65°N for (a) 2010C–CTL and (b) 2090C–CTL. Light (dark) shading indicates significance at the 90% (95%) significance level: contour interval 30 m.

signal is from an ensemble average. It highlights that the polar vortex is more susceptible to be weakened in late winter in 2010C, but the exact timing and amplitude of the signal are quite variable from one ensemble member to another (not shown). The same kind of response was previously obtained by prescribing snow cover (e.g., Fletcher et al. 2009; Peings et al. 2012), surface albedo (Allen and Zender 2010), or tropical Pacific SST (Manzini et al. 2006) perturbations in AGCMs. The 2010C experiment suggests that the observed Arctic sea ice anomalies from recent years also force such a response in late winter. Note that the changes in snow cover (and in land surface albedo) are weak in the perturbation experiments. The response is therefore not related to snow anomalies that could be induced by the loss of sea ice (Cohen et al. 2012).

The same diagnosis for 2090C is shown in Fig. 7b. A response similar to the one depicted in Fig. 7a is found during late winter but, despite the stronger sea ice forcing, the response is weaker than in 2010C. It is only significant in the troposphere and does not involve a clear stratosphere–troposphere propagation. Thus, the stratospheric response obtained in 2010C is sensitive to the prescribed anomalies and does not increase with a stronger SIC/SST forcing. Although 2090C exhibits a weaker response in the stratosphere, a stronger response is found in the troposphere. Indeed, positive anomalies of the polar cap geopotential are visible around 500 hPa in December and February, in line with the negative NAM pattern found for the Z_{500} wintertime mean (Fig. 6f).

These different responses of the wintertime NH atmosphere between the two experiments suggest that different mechanisms are at work in 2010C and 2090C. The late winter response in 2010C involving a coupled stratosphere–troposphere mechanism is investigated in the following section, while the tropospheric response found in 2090C is discussed in section 3c.

b. *Mechanisms for the late winter stratospheric response in 2010C*

The Z_{500} response in 2010C in February is depicted in Fig. 8b. It resembles the negative phase of the NAM, but the negative anomalies of the midlatitudes are far greater over the North Pacific sector (where they are significant)

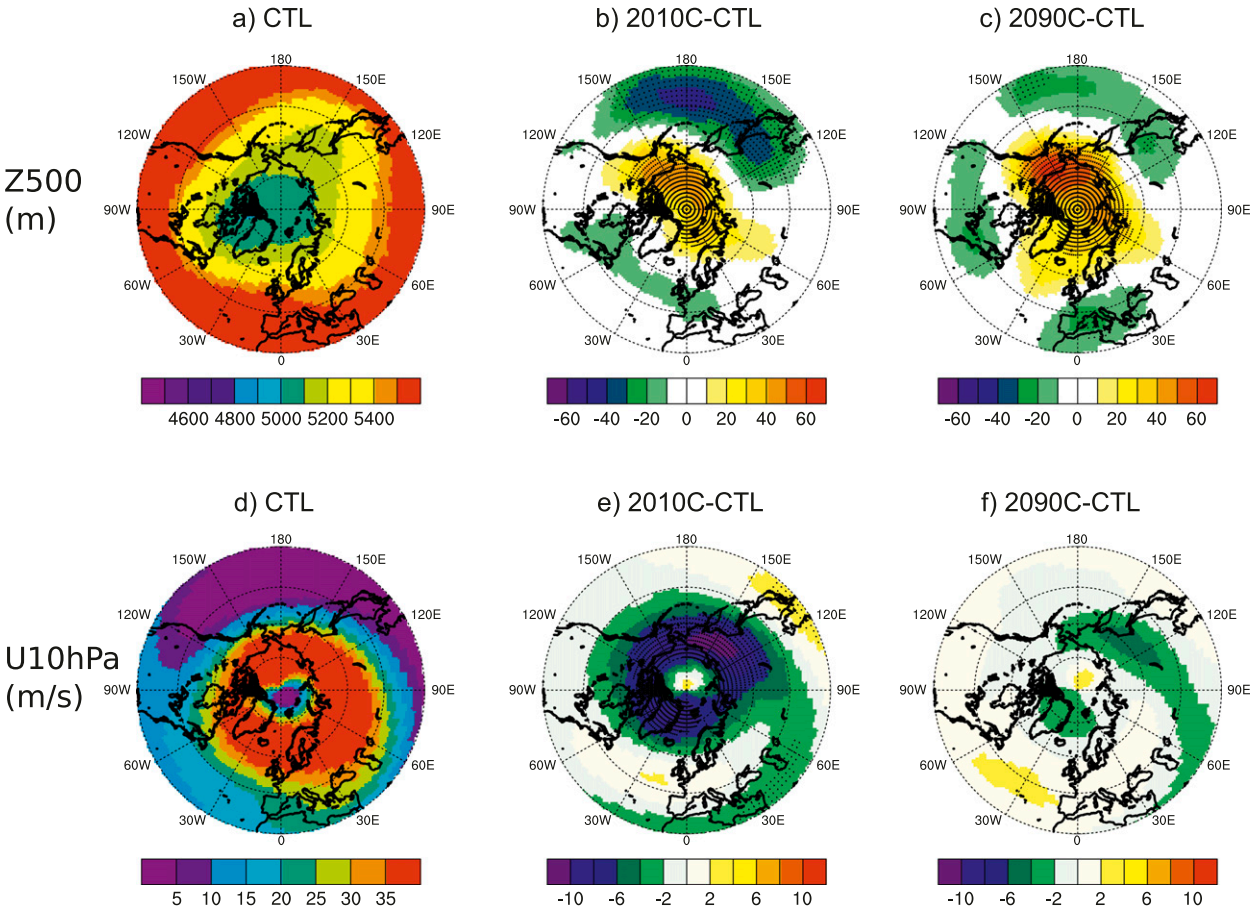

FIG. 8. (a) Mean February 500-hPa geopotential climatology (m) for CTL and the response (b) for 2010C and (c) for 2090C; (d)–(f) as in (a)–(c) but for the 10-hPa zonal wind ($m\,s^{-1}$). Anomalies significant at the 95% confidence level are stippled.

than over the North Atlantic. This strong response of the North Pacific circulation is consistent with the patterns of the SIC/SST and net surface energy flux anomalies (Figs. 2b and 4c). The SIC anomaly in the Sea of Okhotsk, upstream to the North Pacific circulation, has a strong impact on the surface energy budget in late winter (Fig. 4c) and therefore is probably responsible for a large part of the response. This result is also consistent with Honda et al. (1999), who had found that SIC anomalies from the Sea of Okhotsk modified the atmospheric circulation over the North Pacific basin. In line with Fig. 7a, the February response is far greater than that for any other month. This seasonality of the response has been previously reported in similar studies (Magnusdottir et al. 2004; Deser et al. 2007; Seierstad and Bader 2009; Deser et al. 2010), but its cause is unclear. The hemispheric signal is essentially equivalent barotropic (SLP exhibits the same sign anomalies, not shown), in agreement with the late winter response obtained by the previously cited studies. The weakening of the polar vortex, whose climatological values are depicted in Fig. 8d (10-hPa zonal wind, U10 hPa), is clearly visible in Fig. 8e. The maximum response is over eastern Siberia, suggesting that the forcing causing the stratospheric response is located over this region. For the sake of comparison, Figs. 8c and 8f show the February response in 2090C. The Z_{500} pattern resembles the negative phase of the NAM (Fig. 8c), but no significant response is found in the stratosphere (Fig. 8f).

To understand the stratospheric response in 2010C, we look at wave–mean flow interactions by using a wave activity flux diagnostic. We use the Plumb flux (Plumb 1985), valid for quasigeostrophic perturbations, to describe planetary wave propagation in three dimensions. When averaged zonally, this diagnostic is identical to the Eliassen–Palm (EP) flux (Edmon et al. 1980). The horizontal component of the EP flux is proportional to the meridional eddy momentum transport, and the vertical component is proportional to the meridional eddy heat transport. The divergence of the EP flux is a measure of

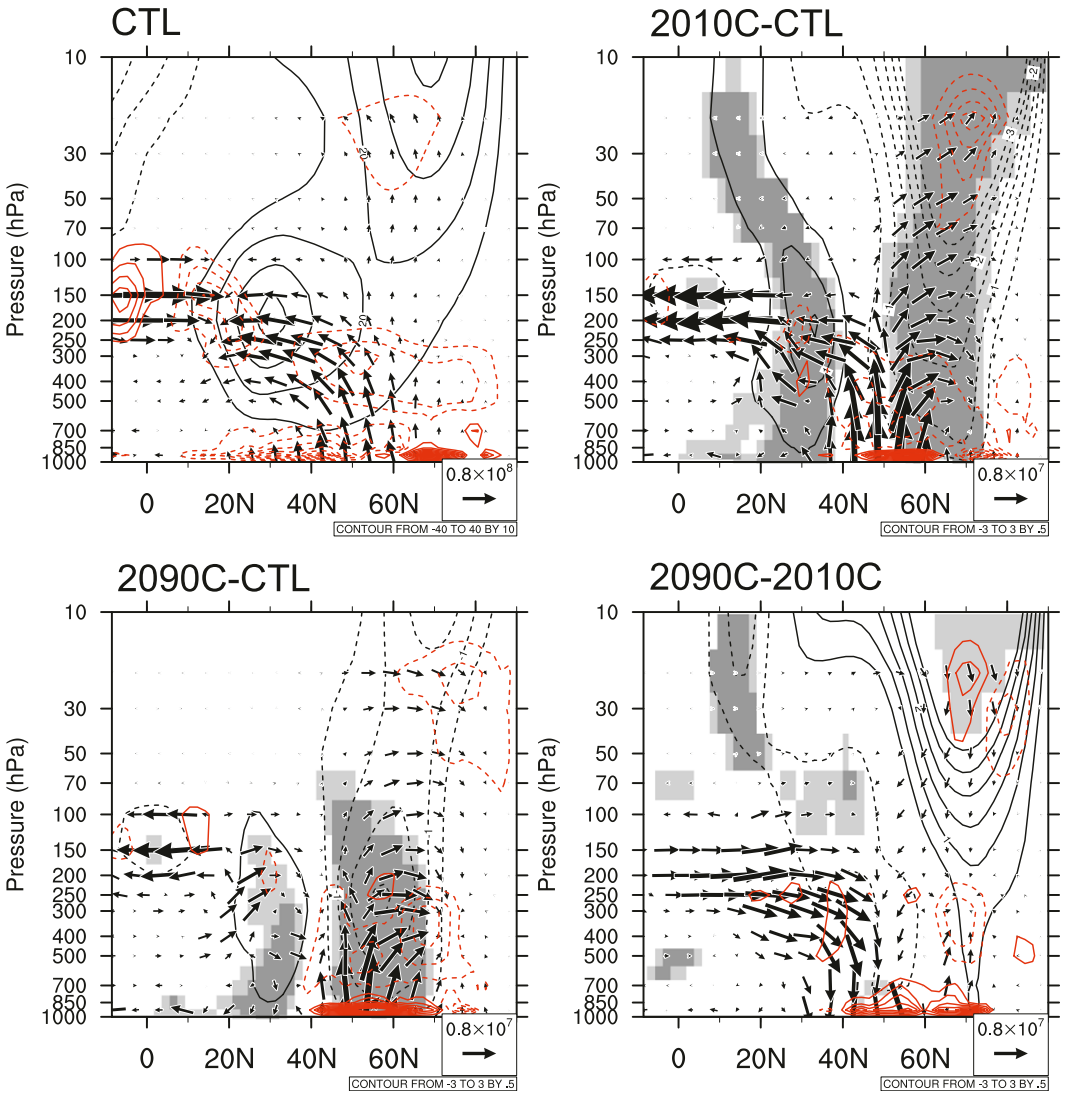

FIG. 9. (a: top left) Zonally averaged zonal wind (black contours, interval 10 m s^{-1}), EP flux (vectors, kg s^{-2}), and EP flux divergence (red contours, interval 1 m s^{-1} day^{-1}) averaged over February in CTL. (b: top right) Response for 2010C (interval for wind is 0.5 m s^{-1}; interval for divergence is 0.3 m s^{-1} day^{-1}). Light (dark) shading indicates the 90% (95%) significance level for zonal wind anomalies. (c: bottom left) As in (b) but for 2090C. (d: bottom right) Difference between the two responses (2090C − 2010C). For display, the meridional and vertical components of the EP flux are multiplied by the square root of p [p = pressure (1000 hPa)$^{-1}$], and the vertical component is multiplied by 100.

the total nondiabatic forcing on the zonal-mean zonal flow with the assumptions of quasigeostrophic theory and linear perturbations [see section 2a in Edmon et al. (1980)]. The zonal-mean zonal flow is accelerated (decelerated) where there is divergence (convergence) of the EP flux. Figure 9a shows the EP flux (arrows), the EP flux divergence (red contours), and the zonal-mean zonal wind (black contours) for CTL in February. The response in the same fields for 2010C is shown in Fig. 9b and for 2090C in Fig. 9c. The climatological westerly zonal flow around 60°N (Fig. 9a) is decelerated over the entire atmospheric column in 2010C (Fig. 9b), while positive anomalies are found in the region of the subtropical jet. The signal associated with the weakening of the polar vortex propagates from the stratosphere to the surface and is associated with an increase in upward EP flux north of 30°N. The anomalous wave activity interacts with the zonal-mean zonal flow, especially in the polar stratosphere where there is convergence of the EP flux and deceleration of the westerly wind (Fig. 9b).

Figure 10 shows the response in the vertical component of the Plumb flux on the 850-hPa level over the

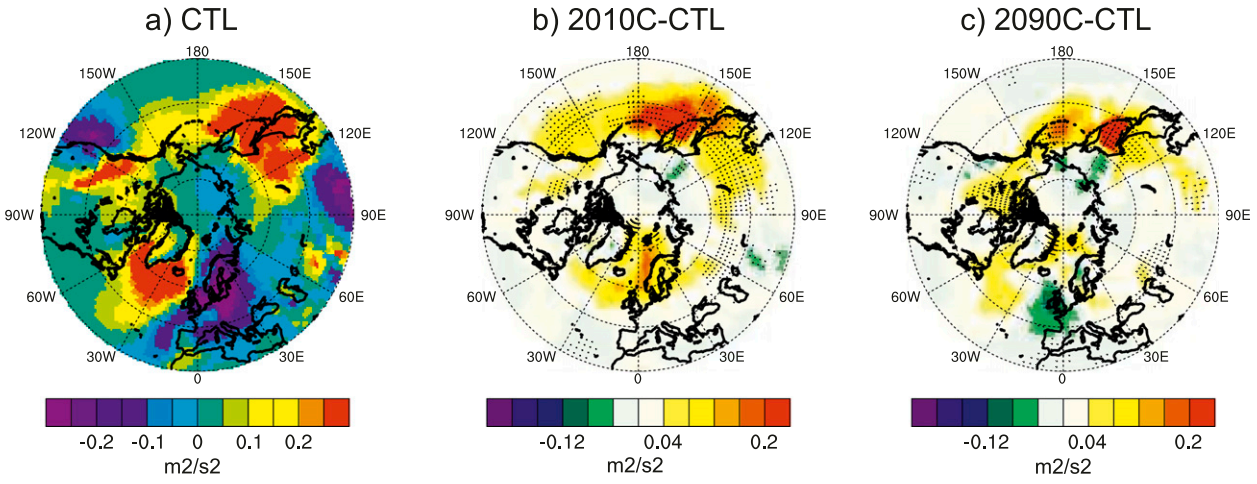

FIG. 10. (a) Mean February vertical component of the Plumb flux at 850 hPa ($m^2 s^{-2}$) for CTL; response (b) for 2010C and (c) for 2090C. Anomalies significant at the 95% confidence level are stippled.

Northern Hemisphere. The location of the maximum vertical flux response is over the North Pacific (Fig. 10b), which might be expected from the strong surface energy flux anomalies over the Sea of Okhotsk (Fig. 4c). It is located in a source region of climatological stationary waves forced by orography and the thermal land–sea contrast (Plumb 1985) that is well represented in our model (Fig. 10a). A secondary area of positive response in the vertical component of the Plumb flux is located over the North Atlantic, especially off the Norwegian coast (Fig. 10b). This signal does not correspond directly to a surface flux response (Fig. 4b) but, considering the large zonal scale of the waves involved, may be an essential part for the remote response. Thus, the SIC/SST anomalies prescribed in 2010C, including those from the Sea of Okhotsk, enhance the climatological upward Plumb flux and lead to a weakening of the stratospheric polar vortex owing to interactions of these anomalous waves with the zonal-mean flow. Concerning 2090C, the EP flux response is qualitatively similar (Fig. 9c) but not as strong as in 2010C (Fig. 9d). The upward Plumb flux over Siberia, the North Pacific, and North Atlantic has a weaker amplitude and less spatial extent (Fig. 10c). With less wave excitation and less convergence of EP flux in the stratosphere (Fig. 9d), the zonal-mean circulation is therefore not as perturbed in 2090C as in 2010C. The negative zonal wind anomalies are only significant in the troposphere, with less impact on the stratospheric polar vortex.

The weaker response in the experiment with the stronger overall forcing, as well as the strong seasonality of the response, deserves to be clarified. Recent studies have emphasized the importance of the linear interference between the forced and climatological waves to obtain a significant response of the NAM (Garfinkel et al. 2010; Smith and Kushner 2012). These works suggest that the phase of the anomalous waves resulting from the external forcing is critical for getting a significant impact on the atmospheric circulation. When the forced wave is in phase with the climatological standing wave (constructive interference), the atmospheric response is stronger than when the forced and climatological waves are out of phase (destructive interference). Thus, not only is the amplitude of the planetary wave response important, but also its phase. This hypothesis has been verified with different surface forcings: tropical SSTs (Fletcher and Kushner 2011), Eurasian snow cover (Smith et al. 2011), and the same can be expected from sea ice forcing. To verify whether the linear interference is critical for explaining the 2010C response in February, the anomalous stationary waves at 60°N attributed to the forcing are plotted in the Fig. 11 (black contours) along with the climatological stationary waves of CTL (color shading) for 2010C (on left) and 2090C (on right). A Fourier decomposition is applied to the monthly geopotential field to decompose the stationary waves according to zonal wavenumber. The results are shown for the raw field (total wave, Fig. 11a), as well as for wave 1 (Fig. 11b) and wave 2 (Fig. 11c), as these wavenumbers correspond to the large spatial scale that can propagate into the stratosphere. The spatial correlation between the forced and climatological components is indicated on the upper right of the panels. In the two experiments, the forced and climatological waves are in phase ($R = 0.44$ and $R = 0.4$ for total wave, Fig. 11a). The phasing is higher over the North Pacific, especially for 2010C ($R = 0.75$ if the spatial correlation is computed over the North Pacific sector, $R = 0.6$ in 2090C) in line with the significant response

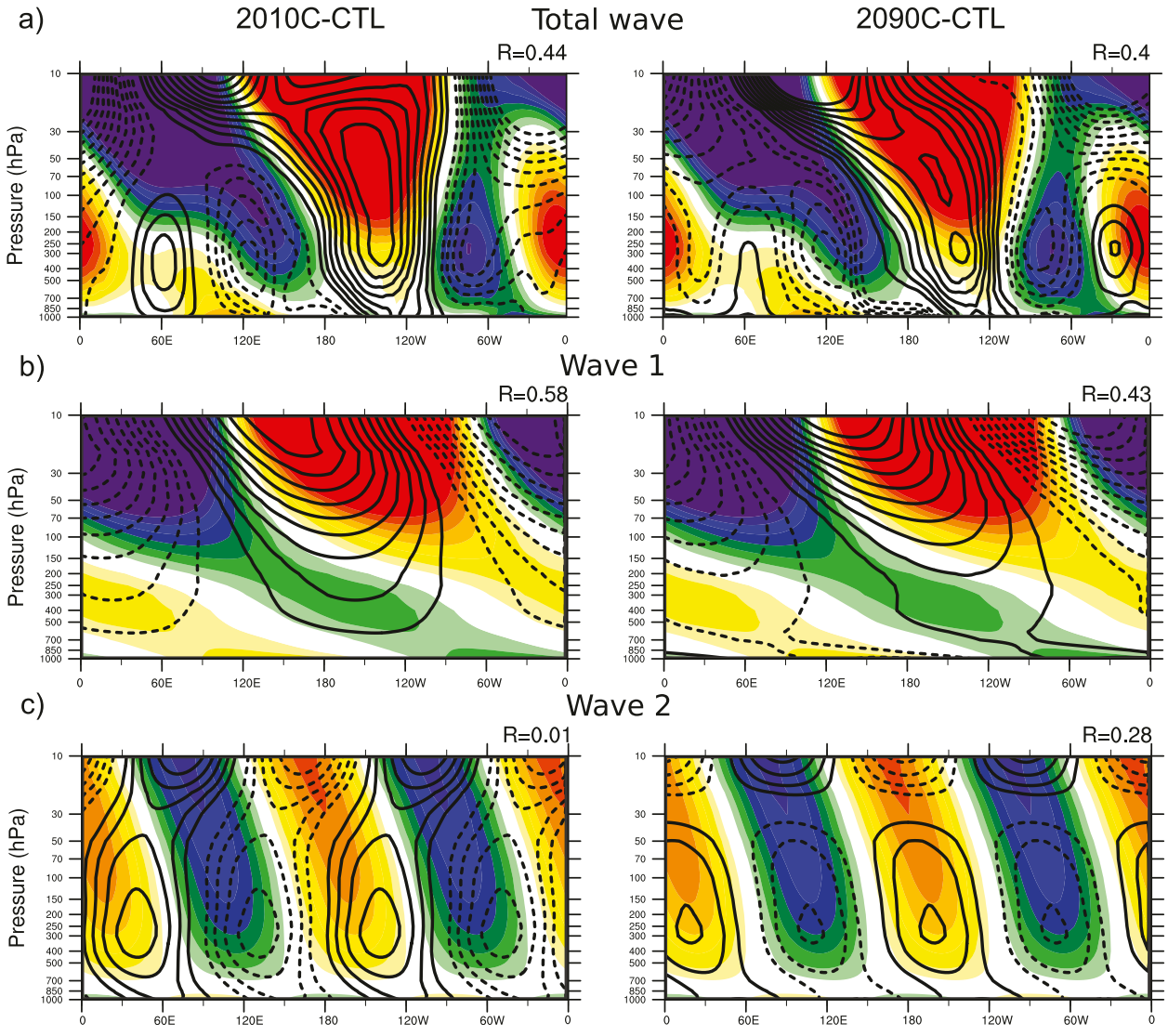

FIG. 11. Forced (contours) and climatological (shading) stationary waves at 60°N in (left) 2010C and (right) 2090C in February. The stationary waves are obtained by removing the zonal mean of the geopotential height. Results are shown in a pressure vs longitude plot for (a) total wave (no Fourier decomposition), (b) zonal wavenumber 1, and (c) zonal wavenumber 2. Spatial correlations between the forced and climatological waves are indicated. Contour interval is 20 m (5 m) for the climatological (forced) waves.

obtained in February in this experiment (Fig. 9b). The overall correlation is also higher in 2010C for wave 1 (Fig. 10b, $R = 0.58$ instead of $R = 0.43$ in 2090C). Concerning wave 2, the phasing is low in both experiments (Fig. 10c). These results suggest that the anomalous surface-forced planetary wave is more likely to propagate into the stratosphere in 2010C. However, the correlations only differ by 0.15 such that the increased propagation of the forced wave in 2010C can hardly be attributed only to linear interference of planetary waves. On the other hand, this diagnostic gives quite a plausible explanation for the seasonality of the response. The forced wave (total wave and wave 1) is out of phase with the climatological equivalent in December and January in the 2010C experiment (not shown, $R = -0.55$ for total wave and $R = -0.9$ for wave 1 in December; $R = -0.33$ for total wave and $R = -0.75$ for wave 1 in January). Thus, destructive interferences in December–January are probably preventing the SIC/SST forcing from modifying the atmospheric circulation in the same way as in February.

In summary, the late winter response in 2010C is related to dynamical processes involving stationary wave-mean flow interactions and a stratospheric pathway. The response is at its maximum in February, when the forced planetary waves interact constructively with the climatological waves, especially over the North Pacific. The

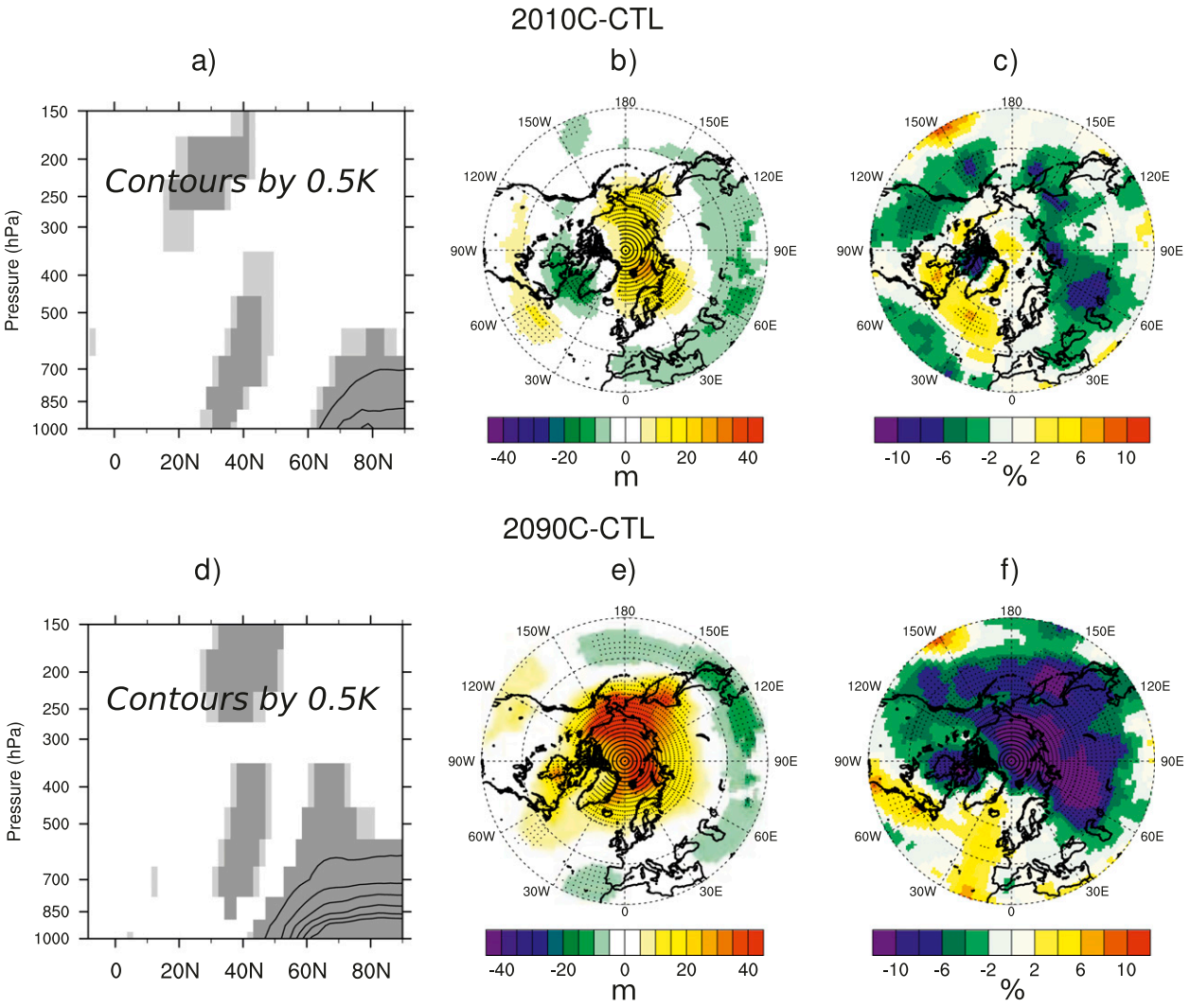

FIG. 12. (a) Zonal mean DJF temperature response (K) in 2010C: contour interval 0.5 K; light (dark) shading indicates the 90% (95%) significance level. (b) Response of the DJF atmospheric thickness between 1000 and 500 hPa (m) in 2010C. (c) Response of the DJF transient activity in 2010C in percent of the climatology. The transient activity is derived from the standard deviation of the 2–6-day bandpass-filtered Z_{500}. Anomalies significant at the 95% confidence level are stippled. (d)–(f) As in (a)–(c) but for 2090C.

spatial distribution of the anomalies is important for obtaining this signal since the greater overall decline of sea ice in 2090C does not lead to a stronger response in the stratospheric polar vortex.

c. *Mechanisms for the winter tropospheric response in 2090C*

Section 3b showed that the late winter response in the stratosphere is weaker in 2090C than in 2010C. However, the overall tropospheric response is greater in this experiment. First, the tropospheric anomalies are hemispheric and not limited to the North Pacific (Fig. 8c). Secondly, they do not occur only in February (Fig. 7b). This result can be attributed to the greater high-latitude warming that occurs not only at the surface (Fig. 5d), but also at upper levels in the troposphere in 2090C. The vertical profile of the temperature response in the perturbation experiments is shown in Fig. 12 for the winter season (DJF). The high-latitude surface warming is greater in 2090C than in 2010C and is significant up to the 500-hPa level (Fig. 12a and 12d). This leads to increased thickness of the lower troposphere (Figs. 12b,e), a phenomenon detected in observations over the past 10 years (Francis and Vavrus 2012). The thermal expansion of the Arctic troposphere reduces the meridional temperature and thickness gradients from the pole to midlatitudes, resulting in a weaker westerly flow around the baroclinic zone in line with the thermal wind arguments.

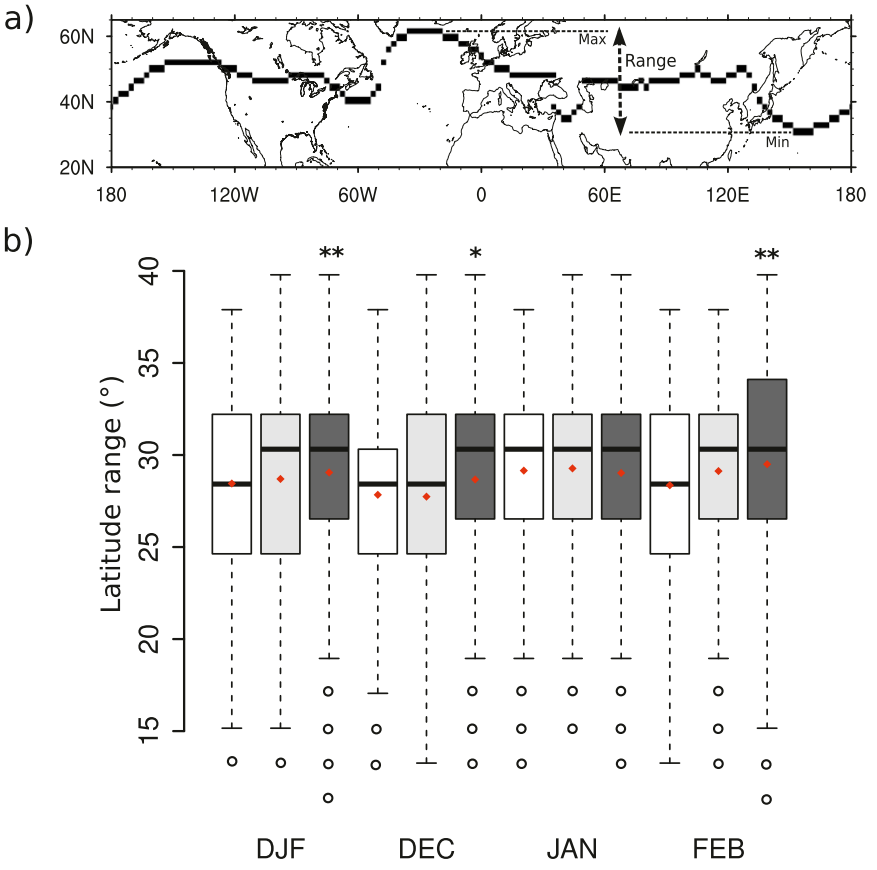

FIG. 13. (a) Example of the latitudinal position of the 5400-m isopleth along longitude for one day of February in CTL. The minimum, maximum, and range of the latitudinal positions are indicated. (b) Distribution of the daily ranges (° lat) of the 5400-m isopleth for CTL (white boxplots), 2010C (light gray boxplots), and 2090C (dark gray boxplots) in winter (DJF). Boxplots and whiskers indicate the maximum, upper quartile, median, lower quartile, and minimum of the distribution (horizontal bars). Outliers are represented by circles. The mean of the distribution is shown by red diamonds, and asterisks indicate the significance level of the change of the mean in 2010C and 2090C, compared to the CTL value (*: $p < 0.1$; **: $p < 0.05$, according to a Student's t test applied on the seasonal means of the range; see text).

The reduced westerly flow in the troposphere, visible in the 2090C experiment (Fig. 9c), favors the intrusion of air from the midlatitudes toward the pole (or cold air intrusion from the pole to midlatitudes) and the negative phase of the NAM.

A significant decrease in transient activity is also found in both experiments, especially over the Arctic, Siberia, and the North Pacific in 2090C (Figs. 12c,f). The transient activity is derived from the standard deviation of the 2–6-day bandpass-filtered Z_{500}. The resulting change in the transient eddy momentum flux feedbacks positively with the anomalies of the zonal mean circulation, as reported in previous studies (Deser et al. 2007; Seierstad and Bader 2009). The tropospheric response in 2090C is thus driven by a thermodynamic effect over the Arctic that is likely reinforced by the feedback of baroclinic eddies onto the zonal mean circulation.

d. Is there an increase of extremes over midlatitudes?

We first examine whether a change in the wintertime meridional amplitude of planetary waves is detectable over the midlatitudes in our set of experiments (Francis and Vavrus 2012; Screen and Simmonds 2013). A method close to the one of Screen and Simmonds is used. For each day in winter, the range of the 5400-m isopleth on the 500-hPa pressure surface is computed as the difference between the maximum and minimum latitude of the isopleth over all longitudes. One example of a meander (for one day of February in CTL) is shown in Fig. 13a, with a schematic view of the daily range. While Screen and Simmonds (2013) focused on the seasonal mean of the ranges, we focus on the distribution of the daily ranges in each of our experiments. The distributions of the daily ranges of the 5400-m isopleth are shown in

Fig. 13b for the entire winter (DJF) and individual months (white boxplots for CTL, light gray boxplots for 2010C, and dark gray boxplots for 2090C). In addition to the median, upper and lower quartiles, maximum and minimum, the mean value of the range (indicated by the red diamond), and the outliers of the distribution (circles) are represented. The asterisks indicate significant difference with CTL in the mean of the distribution using a Student's t test. The t test is applied on the seasonal mean of daily ranges and not directly on daily ranges, so as to have a set of independent values (50 values). For the entire season (DJF) there is not a significant change of the mean range in 2010C. However, a slight increase is detected in February, even though it is not significant at the 90% confidence level ($p = 0.11$). Moreover, the distribution shifts toward positive values (increase of the median), especially in February. The changes in 2090C are qualitatively the same as in 2010C but with a larger amplitude. The DJF mean of wave amplitude increases in 2090C (signal significant to the 95% confidence level). This signal is due to significant increases in the December mean ($p < 0.1$) and February mean ($p < 0.05$), in line with the strongest signal found in the troposphere during these months (Fig. 7b). As for 2010C, no significant change is detected in January. Except for the upper quartile, the entire DJF distribution is shifted toward higher-latitude ranges in 2090C, with an increase in the median, the lower quartile, and the minimum and maximum values.

A Fourier decomposition similar to Screen and Simmonds (2013) has been applied to daily Z_{500} in order to isolate the role of each of the five first zonal wavenumbers ($k = 1$ to 5) in the overall response. Moreover, the analyses have been repeated on the four sectors of longitude that they use: Atlantic Ocean/Europe (−60°W–60°E), Eurasia/west Pacific (60°E–180°), east Pacific/North America (−180°–60°W), and North America/North Atlantic (−140°W–0°). We do not show the results of these analyses, but they reveal that wave-1 is the major contributor to the response shown in Fig. 13b, and the amplitude of the signal is stronger over Eurasia. We emphasize that these effects have small values (only 1° to 2° latitude change in the range), such that they do not constitute a strong influence from Arctic sea ice change on the meanders of planetary waves in midlatitudes. However, they are significant according to our statistical test, and the tendency toward larger north–south amplitude of the planetary waves supports the hypothesis of Francis and Vavrus (2012).

To explore whether a change in extremes of cold temperatures over midlatitudes is also detectable in our experiments, Fig. 14 shows the 10th percentile of the surface temperature (at the 1000-hPa level, the daily 2-m temperature was not available for these experiments). It is computed at each grid point from the daily data of the 50 ensemble members of our experiments for DJF and the individual months. In 2010C, the current Arctic SIC/SST forcing increases the intensity of cold extremes over Asia. Indeed, the pattern of the DJF response (Fig. 14a) is similar to that obtained for the mean temperature response (Fig. 5b) but with a larger amplitude of the cooling over the midlatitudes in Asia from the Caspian Sea to the Pacific coast during all winter months (Figs. 14b,c,d). The same response is not found over Europe and North America, except in February when the negative phase of the NAM is favored in 2010C (Fig. 14d). Conversely, the intensity of cold extremes is reduced in the vicinity of the surface warming associated with less sea ice, especially over Scandinavia and eastern Europe. In 2090C, the large warming spreads beyond the Arctic into midlatitudes and decreases the intensity of cold extremes north of 45°N during all of winter (Figs. 14e,f,g,h). South of 45°N the increase of cold extremes over Asia persists but is not greater than in 2010C. The only increase of cold extremes in 2090C compared to 2010C is located in February over Europe and North America (Fig. 14h), consistent with the negative NAM and the elongation of the midlatitude meanders during this month (Figs. 7b and 13b).

In summary, these analyses support the idea that current Arctic sea ice conditions (2010C) favor the intensity of cold extremes over midlatitudes, although in our model the effect is mostly limited to the Asian sector. When the SIC/SST forcing is stronger (2090C), the intensity of cold extremes decreases everywhere north of 45°N owing to the extension of the Arctic warm anomaly over the northern continents. In 2090C (as in 2010C), cold extremes are more intense south of 45°N. However, despite far greater warming over the Arctic in 2090C, the intensity of cold extremes does not increase much compared to 2010C. This nonlinear relationship between SIC retreat and midlatitude temperature is consistent with Petoukhov and Semenov (2010), who have identified similar nonlinearity in their model, although their study was limited to the effect of sea ice over the Barents and Kara Seas.

4. Discussion and conclusions

In this study, we have documented the response of the latest version of the NCAR atmospheric model, CAM5, to current and projected Arctic sea ice loss. Two 50-member perturbation experiments, initialized from a control run with prescribed SIC/SST from the 1979–2000 period, were performed using outputs from May through the following April. In the first experiment,

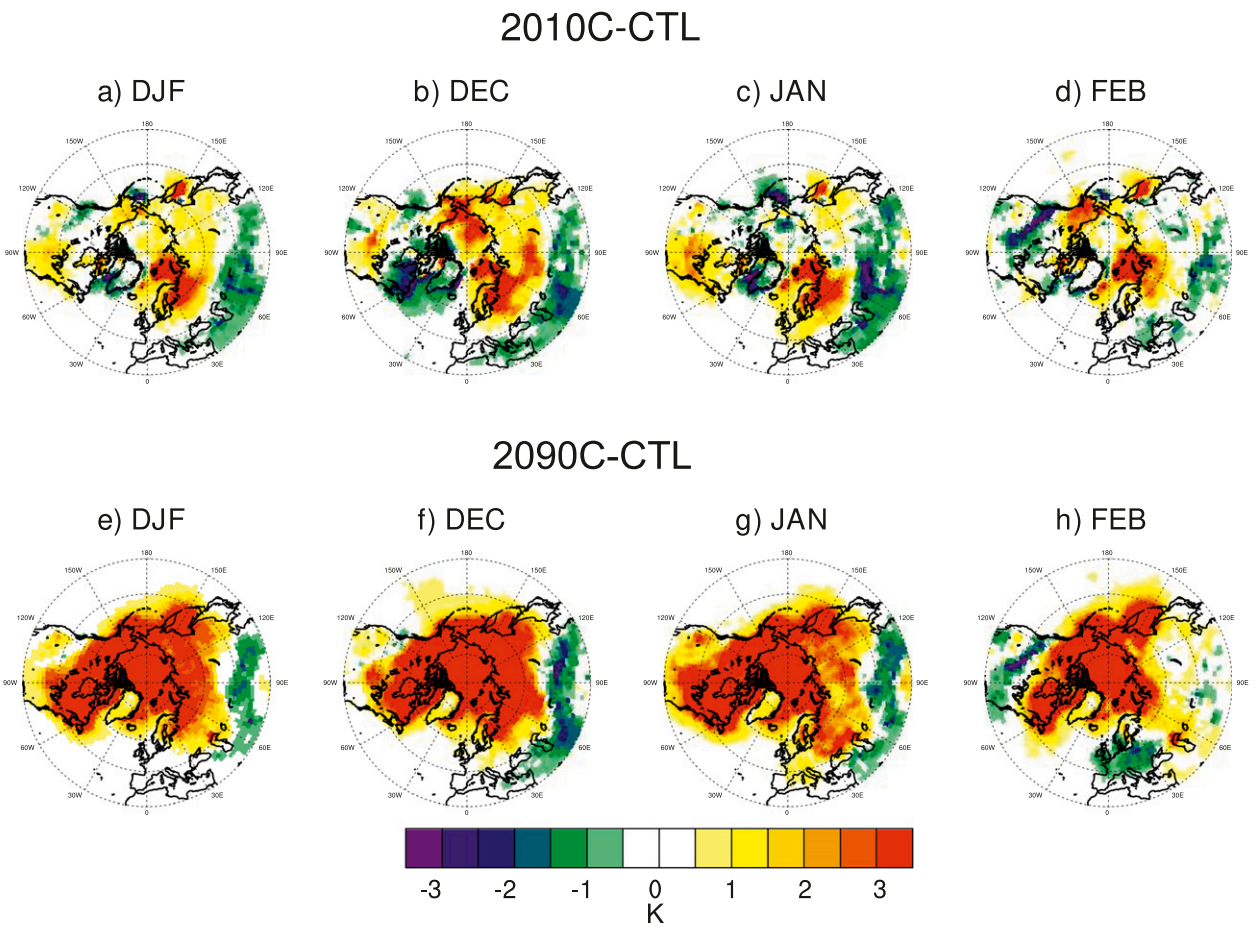

FIG. 14. Response of the 10th percentile of the 1000-hPa daily temperature (K) in 2010C in (a) winter (DJF), (b) December, (c) January, and (d) February; (e)–(h) as in (a)–(d) but for 2090C.

the 2007–12 average annual cycle of Arctic SIC/SST is prescribed to assess the impact of recent sea ice anomalies on the atmospheric circulation. In the second experiment, the annual cycle imposed on the model is representative of the projected SIC/SST conditions at the end of the twenty-first century, taken from a coupled simulation using the RCP8.5 scenario of anthropogenic emissions.

This study highlights new findings about the sensitivity of the wintertime NH atmospheric circulation to reduced Arctic sea ice concentration. First, the recent sea ice anomalies force a stratospheric response in late winter (2010C experiment). The surface forcing leads to an enhancement of the NH climatological planetary waves. The anomalous waves propagate into the stratosphere where they weaken the polar vortex through wave–mean flow interaction, then the polar cap anomaly propagates downward and reaches the surface a few weeks later, in line with the timing of the stratosphere–troposphere mechanisms observed in nature (Baldwin and Dunkerton 2001; Christiansen 2001). The response in the troposphere and at the surface is greater over the North Pacific, suggesting the importance of the anomalies from the Sea of Okhotsk. The planetary wave propagation is maximum in late winter when positive interference between the forced waves and the climatological stationary waves can take place. Wave number one is the most important in this process. It is not clear why the forced and climatological waves are only in phase during late winter and not earlier in the season. This is probably related to the pattern of sea ice anomalies and to the evolution of the background zonal flow. This question deserves further investigation. The late winter response projects onto the negative phase of the NAM in the troposphere and favors cold conditions over midlatitudes (mostly over Asia in our results). We find that the current sea ice decline leads to an increase in the meridional meander of midlatitude planetary waves, but the statistical significance of this signal is low, as it is in observations (Francis and Vavrus 2012; Screen and Simmonds 2013).

The 2010C experiment can be compared directly to the study of Screen et al. (2013b) owing to the similarity

in the sea ice forcing and the use of a previous version of the same atmospheric model (CAM3 instead of CAM5). The main difference in the results of the two studies concerns the late winter response: they identified a weak strengthening of the stratospheric polar vortex, while we find a substantial weakening of the polar vortex and then a downward propagation of this signal to the surface. The difference in response can be related to many factors since numerous modifications have been made in the current version of the model. The new representation of aerosols and clouds in CAM5 is one of the major new features and it may explain some of the differences between the two studies. Clouds in particular may be important since the new model has a different annual cycle of the Arctic cloud cover (Kay et al. 2012b). Indeed, the representation of clouds in climate models is critical for explaining future Arctic climate response (Kay et al. 2012a).

A stronger sea ice forcing is imposed in 2090C, with a different spatial distribution of the anomalies (2090C shows an extensive ice loss within the Arctic basin where none exists in 2010C, and the east–west dipole patterns of sea ice change within the Atlantic and Pacific basins in 2010C are replaced by ice loss in 2090C). This different sea ice forcing leads to a different response of the NH atmospheric circulation. The late winter stratospheric response in 2090C is considerably weaker than in 2010C, with a somewhat less constructive interference between the forced and climatological stationary waves than in 2010C. The tropospheric response in 2090C has a stronger NAM-type response for DJF than in 2010C. This result is in agreement with previous studies that showed that a strong decrease of Arctic sea ice favors the negative phase of the NAM in winter (Seierstad and Bader 2009; Deser et al. 2010). However, the response is quite baroclinic over the Arctic in our model such that the pattern at the surface is not typical of a NAM pattern, except in February. The hemispheric response in 2090C is driven by the significant warming of the polar lower troposphere, extending from the surface to 500 hPa. The thermal expansion of the atmosphere decreases the meridional gradient of atmospheric thickness between the pole and midlatitudes, leading to a weakening of the zonal westerly flow. This thermodynamic effect is reinforced by the feedback of baroclinic eddies onto the zonal mean circulation. Another important finding from this experiment is that the intensity of cold extremes over midlatitudes does not increase linearly with the loss of sea ice. A weak but significant change is found regarding the meridional amplitude of the midlatitude planetary waves, in agreement with the findings of Francis and Vavrus (2012), especially in February and over Eurasia. However, the cold extremes do not increase more in 2090C than in 2010C owing to the large lower-tropospheric warming that extends well beyond the Arctic and prevents the occurrence of cold episodes (except in February when the NAM response is larger). This result supports the study by Petoukhov and Semenov (2010) that identified a nonlinear relationship between the Arctic sea ice loss and cooling of the midlatitudes. It tempers the conclusions of Tang et al. (2013) that expect an increase in cold winter extremes in the twenty-first century with the decline of Arctic sea ice, based on recent observations.

According to our simulations, the response of midlatitude land surface temperatures to sea ice loss depends on the strength of the thermodynamic effect, which is dominant in 2090C compared to the dynamical response identified in late winter in 2010C. Based on this latter experiment, the recent sea ice decline may have favored the negative NAM and the cold temperatures observed over the last winters (Cattiaux et al. 2010; Coumou and Rahmstorf 2012; Cohen et al. 2012). However, this dynamical response is weaker when the model is forced with the projected 2080–99 sea ice, and it is offset by the large warming of the polar and midlatitude regions that limit the intensity of cold extreme temperatures. The balance between these two effects is thus important when determining the range of sea ice loss that favors cold conditions over midlatitudes and the threshold beyond which warmer conditions may be expected in winter. Both thermodynamical and dynamical effects due to sea ice removal may be simulated only approximately in our model. Moreover, it is possible that the projected sea ice concentration of the 2080–99 period used in this study could be reached earlier in the twenty-first century (Overland and Wang 2013). Therefore, further work using observations and numerical experiments will be necessary to confirm the existence in nature of the mechanisms identified in this paper.

This study has focused on the role of sea ice forcing on the atmospheric circulation, but the sea ice decline is only one aspect of the Arctic amplification process. In particular, we did not take into account the role of anthropogenic forcing (identical in all our simulations and representative of year 2000) that drives the Arctic amplification not only through sea ice loss, but also through changes in snow cover, water vapor, clouds, and so on. This is not critical for the 2010C experiment since the prescribed greenhouse gas/aerosol concentrations are close to those from the 2007–12 period. However, the warming of the Arctic region is probably underestimated in 2090C, whereby the atmospheric response revealed in this experiment is likely a lower bound on the actual response with increasing

greenhouse gases. Furthermore, the changes in sea ice thickness were not included due to the lack of sufficient observations. The response might be different with a thinner ice that allows more heat exchange between the ocean and the atmosphere. The importance of oceanic feedback (using simulations with an interactive ocean) also remains to be quantified. Such efforts will help to improve our understanding of interactions between the atmosphere and Arctic sea ice and will allow us to better anticipate the fate of wintertime conditions over the Northern Hemisphere in the next decades.

Acknowledgments. This work was supported by NSF Grant AGS-1206120 and NOAA Grant NA09OAR4310132. We thank the three anonymous reviewers for helpful comments and suggestions on the manuscript. We also acknowledge high-performance computing support from Yellowstone (http://n2t.net/ark:/85065/d7wd3xhc) provided by NCAR's Computational and Information Systems Laboratory, sponsored by the National Science Foundation.

REFERENCES

Alexander, M., U. Bhatt, J. Walsh, M. Timlin, J. Miller, and J. Scott, 2004: The atmospheric response to realistic Arctic sea ice anomalies in an AGCM during winter. *J. Climate,* **17,** 890–905.

Allen, R. J., and C. S. Zender, 2010: The effects of continental-scale snow albedo anomalies on the wintertime Arctic Oscillation. *J. Geophys. Res.,* **115,** D23105, doi:10.1029/2010JD014490.

Baldwin, M. P., and T. J. Dunkerton, 2001: Stratospheric harbingers of anomalous weather regimes. *Science,* **294,** 581–584.

——, and D. W. J. Thompson, 2009: A critical comparison of stratosphere-troposphere coupling indices. *Quart. J. Roy. Meteor. Soc.,* **135,** 1661–1672.

Balmaseda, M. A., L. Ferranti, F. Molteni, and T. N. Palmer, 2010: Impact of 2007 and 2008 Arctic ice anomalies on the atmospheric circulation: Implications for long-range predictions. *Quart. J. Roy. Meteor. Soc.,* **136,** 1655–1664, doi:10.1002/qj.661.

Bhatt, U., M. Alexander, C. Deser, J. Walsh, J. Miller, M. Timlin, J. Scott, and R. Tomas, 2008: The atmospheric response to realistic reduced summer Arctic sea ice anomalies. *Arctic Sea Ice Decline: Observations, Projections, Mechanisms, and Implications, Geophys. Monogr.,* Vol. 180, Amer. Geophys. Union, 91–110.

Blüthgen, J., R. Gerdes, and M. Werner, 2012: Atmospheric response to the extreme Arctic sea ice conditions in 2007. *Geophys. Res. Lett.,* **39,** L02707, doi:10.1029/2011GL050486.

Budikova, D., 2009: Role of Arctic sea ice in global atmospheric circulation: A review. *Global Planet. Change,* **68,** 149–163, doi:10.1016/j.gloplacha.2009.04.001.

Cassano, E. N., J. J. Cassano, M. E. Higgins, and M. C. Serreze, 2013: Atmospheric impacts of an Arctic sea ice minimum as seen in the Community Atmosphere Model. *Int. J. Climatol.,* doi:10.1002/joc.3723, in press.

Cattiaux, J., and C. Cassou, 2013: Opposite CMIP3/CMIP5 trends in the wintertime northern annular mode explained by combined local sea ice and remote tropical influences. *Geophys. Res. Lett.,* **40,** 3682–3687, doi:10.1002/grl.50643.

——, R. Vautard, C. Cassou, P. Yiou, V. Masson-Delmotte, and F. Codron, 2010: Winter 2010 in Europe: A cold extreme in a warming climate. *Geophys. Res. Lett.,* **37,** L20704, doi:10.1029/2010GL044613.

Christiansen, B., 2001: Downward propagation of zonal mean zonal wind anomalies from the stratosphere to the troposphere: Model and reanalysis. *J. Geophys. Res.,* **106** (D21), 27 307–27 322.

Cohen, J. L., J. C. Furtado, M. A. Barlow, V. A. Alexeev, and J. E. Cherry, 2012: Arctic warming, increasing snow cover and widespread boreal winter cooling. *Environ. Res. Lett.,* **7,** 014007, doi:10.1088/1748-9326/7/1/014007.

Comiso, J. C., C. L. Parkinson, R. Gersten, and L. Stock, 2008: Accelerated decline in the Arctic sea ice cover. *Geophys. Res. Lett.,* **35,** L01703, doi:10.1029/2007GL031972.

Coumou, D., and S. Rahmstorf, 2012: A decade of weather extremes. *Nat. Climate Change,* **2,** 491–496.

Deser, C., J. E. Walsh, and M. S. Timlin, 2000: Arctic sea ice variability in the context of recent atmospheric circulation trends. *J. Climate,* **13,** 617–633.

——, G. Magnusdottir, R. Saravanan, and A. Phillips, 2004: The effects of North Atlantic SST and sea ice anomalies on the winter circulation in CCM3. Part II: Direct and indirect components of the response. *J. Climate,* **17,** 877–889.

——, R. A. Tomas, and S. Peng, 2007: The transient atmospheric circulation response to North Atlantic SST and sea ice anomalies. *J. Climate,* **20,** 4751–4767.

——, A. S. Phillips, and M. A. Alexander, 2010: Twentieth century tropical sea surface temperature trends revisited. *Geophys. Res. Lett.,* **37,** L10701, doi:10.1029/2010GL043321.

Edmon, H. J., B. J. Hoskins, and M. E. McIntyre, 1980: Eliassen-Palm cross sections for the troposphere. *J. Atmos. Sci.,* **37,** 2600–2616.

Fletcher, C. G., and P. J. Kushner, 2011: The role of linear interference in the annular mode response to tropical SST forcing. *J. Climate,* **24,** 778–794.

——, S. C. Hardiman, P. J. Kushner, and J. L. Cohen, 2009: The dynamical response to snow cover perturbations in a large ensemble of atmospheric GCM integrations. *J. Climate,* **22,** 1208–1222.

Francis, J., and S. Vavrus, 2012: Evidence linking Arctic amplification to extreme weather in mid-latitudes. *Geophys. Res. Lett.,* **39,** L06801, doi:10.1029/2012GL051000.

——, W. Chen, D. Leathers, J. Miller, and D. Veron, 2009: Winter Northern Hemisphere weather patterns remember summer Arctic sea-ice extent. *Geophys. Res. Lett.,* **36,** L07503, doi:10.1029/2009GL037274.

Garfinkel, C. I., D. L. Hartmann, and F. Sassi, 2010: Tropospheric precursors of anomalous Northern Hemisphere stratospheric polar vortices. *J. Climate,* **23,** 3282–3299.

Honda, M., K. Yamazaki, H. Nakamura, and K. Takeuchi, 1999: Dynamic and Thermodynamic characteristics of atmospheric response to anomalous sea ice extent in the Sea of Okhotsk. *J. Climate,* **12,** 3347–3358.

——, J. Inoue, and S. Yamane, 2009: Influence of low Arctic sea-ice minima on anomalously cold Eurasian winters. *Geophys. Res. Lett.,* **36,** L08707, doi:10.1029/2008GL037079.

Kay, J. E., M. Holland, C. Bitz, E. Blanchard-Wrigglesworth, A. Gettelman, A. Conley, and D. Bailey, 2012a: The influence of local feedbacks and northward heat transport on the equilibrium Arctic climate response to increased greenhouse gas forcing. *J. Climate,* **25,** 5433–5450.

——, and Coauthors, 2012b: Exposing global cloud biases in the Community Atmosphere Model (CAM) using satellite observations and their corresponding instrument simulators. *J. Climate,* **25,** 5190–5207.

Kumar, A., and Coauthors, 2010: Contribution of sea ice loss to Arctic amplification. *Geophys. Res. Lett.,* **37,** L21701, doi:10.1029/2010GL045022.

Kurtz, N., T. Markus, S. Farrell, D. Worthern, and L. Boisvert, 2011: Observations of recent Arctic sea ice volume loss and its impact on ocean–atmosphere energy exchange and ice production. *J. Geophys. Res.,* **116,** C04015, doi:10.1029/2010JC006235.

Linkin, M. E., and S. Nigam, 2008: The North Pacific Oscillation–west Pacific teleconnection pattern: Mature-phase structure and winter impacts. *J. Climate,* **21,** 1979–1997.

Liu, J., Z. Zhang, R. M. Horton, C. Wang, and X. Ren, 2007: Variability of North Pacific sea ice and East Asia–North Pacific winter climate. *J. Climate,* **20,** 1991–2001.

——, J. A. Curry, H. Wang, M. Song, and R. M. Horton, 2012: Impact of declining Arctic sea ice on winter snowfall. *Proc. Natl. Acad. Sci. USA,* **109,** 4074–4079, doi:10.1073/pnas.1114910109.

Magnusdottir, G., C. Deser, and R. Saravanan, 2004: The effects of North Atlantic SST and sea ice anomalies on the winter circulation in CCM3. Part I: Main features and storm-track characteristics of the response. *J. Climate,* **17,** 857–876.

Manzini, E., M. A. Giorgetta, M. Esch, L. Kornblueh, and E. Roeckner, 2006: The influence of sea surface temperatures on the northern winter stratosphere: Ensemble simulations with the MAECHAM5 model. *J. Climate,* **19,** 3863–3881.

Matthewman, N. J., and G. Magnusdottir, 2011: Observed interaction between Pacific sea ice and the western Pacific pattern on intraseasonal time scales. *J. Climate,* **24,** 5031–5042.

Neale, R. B., and Coauthors, 2011: Description of the NCAR Community Atmosphere Model (CAM5). National Center for Atmospheric Research Tech. Rep. NCAR/TN-486+STR, 268 pp.

Ogi, M., and J. M. Wallace, 2012: The role of summer surface wind anomalies in the summer Arctic sea ice extent in 2010 and 2011. *Geophys. Res. Lett.,* **39,** L09704, doi:10.1029/2012GL051330.

Orsolini, Y., R. Senan, R. Benestad, and A. Melsom, 2012: Autumn atmospheric response to the 2007 low Arctic sea ice extent in coupled ocean–atmosphere hindcasts. *Climate Dyn.,* **38,** 2437–2448.

Overland, J. E., and M. Wang, 2013: When will the summer Arctic be nearly sea ice free? *Geophys. Res. Lett.,* **40,** 2097–2101, doi:10.1002/grl.50316.

——, J. A. Francis, E. Hanna, and M. Wang, 2012: The recent shift in early summer Arctic atmospheric circulation. *Geophys. Res. Lett.,* **39,** L19804, doi:10.1029/2012GL053268.

Peings, Y., D. Saint-Martin, and H. Douville, 2012: A numerical sensitivity study of the Siberian snow influence on the northern annular mode. *J. Climate,* **25,** 592–607.

Petoukhov, V., and V. Semenov, 2010: A link between reduced Barent-Kara sea ice and cold winter extremes over northern continents. *J. Geophys. Res.,* **115,** D21111, doi:10.1029/2009JD013568.

Plumb, R. A., 1985: On the three-dimensional propagation of stationary waves. *J. Atmos. Sci.,* **42,** 217–229.

Polvani, L. M., and D. W. Waugh, 2004: Upward wave activity flux as a precursor to extreme stratospheric events and subsequent anomalous surface weather regimes. *J. Climate,* **17,** 3548–3554.

Porter, D., J. Cassano, and M. Serreze, 2012: Local and large-scale atmospheric responses to reduced Arctic sea ice and ocean warming in the WRF model. *J. Geophys. Res.,* **117,** D11115, doi:10.1029/2011JD016969.

Rayner, N. A., D. E. Parker, E. B. Horton, C. K. Folland, L. V. Alexander, D. P. Rowell, E. C. Kent, and A. Kaplan, 2003: Global analyses of sea surface temperature, sea ice, and night marine air temperature since the late nineteenth century. *J. Geophys. Res.,* **108** (D14), 4407, doi:10.1029/2002JD002670.

Screen, J. A., and I. Simmonds, 2010: The central role of diminishing sea ice in recent Arctic temperature amplification. *Nature,* **464,** 1334–1337.

——, and ——, 2013: Exploring links between Arctic amplification and mid-latitude weather. *Geophys. Res. Lett.,* **40,** 959–964, doi:10.1002/grl.50174.

——, C. Deser, I. Simmonds, and R. Tomas, 2013a: Atmospheric impacts of Arctic sea-ice loss, 1979–2009: Separating forced change from atmospheric internal variability. *Climate Dyn.,* doi:10.1007/s00382-013-1830-9.

——, I. Simmonds, C. Deser, and R. Tomas, 2013b: The atmospheric response to three decades of observed Arctic sea ice loss. *J. Climate,* **26,** 1230–1248.

Seierstad, I., and J. Bader, 2009: Impact of a projected future Arctic sea ice reduction on extratropical storminess and the NAO. *Climate Dyn.,* **33,** 937–943.

Semmler, T., R. McGrath, and S. Wang, 2012: The impact of Arctic sea ice on the Arctic energy budget and on the climate of the northern mid-latitudes. *Climate Dyn.,* **39,** 2675–2694, doi:10.1007/s00382-012-1353-9.

Serreze, M. C., and J. A. Francis, 2006: The Arctic amplification debate. *Climatic Change,* **76,** 241–264, doi:10.1007/s10584-005-9017-y.

——, M. M. Holland, and J. Stroeve, 2007: Perspectives on the Arctic's shrinking sea ice cover. *Science,* **315,** 1533–1536.

Simmonds, I., and I. Rudeva, 2012: The great Arctic cyclone of August 2012. *Geophys. Res. Lett.,* **39,** L23709, doi:10.1029/2012GL054259.

Singarayer, J., J. Bamber, and P. Valdes, 2006: Twenty-first-century climate impacts from a declining Arctic sea ice cover. *J. Climate,* **19,** 1109–1125.

Smith, K. L., and P. J. Kushner, 2012: Linear interference and the initiation of extratropical stratosphere-troposphere interactions. *J. Geophys. Res.,* **117,** D13107, doi:10.1029/2012JD017587.

——, ——, and J. Cohen, 2011: The role of linear interference in northern annular mode variability associated with Eurasian snow cover extent. *J. Climate,* **24,** 6185–6202.

Solomon, S., D. Qin, M. Manning, Z. Chen, M. Marquis, K. Averyt, M. Tignor, and H. L. Miller Jr., Eds., 2007: *Climate Change 2007: The Physical Science Basis.* Cambridge University Press, 996 pp.

Strey, S., W. Chapman, and J. Walsh, 2010: The 2007 sea ice minimum: Impacts on the Northern Hemisphere atmosphere in

late autumn and early winter. *J. Geophys. Res.,* **115,** D23103, doi:10.1029/2009JD013294.

Stroeve, J. C., M. M. Holland, W. Meier, T. Scambos, and M. Serreze, 2007: Arctic sea ice decline: Faster than forecast. *Geophys. Res. Lett.,* **34,** L09501, doi:10.1029/2007GL029703.

——, M. C. Serreze, M. M. Holland, J. E. Kay, J. Maslanik, and A. P. Barrett, 2011: The Arctic's rapidly shrinking sea ice cover: A research synthesis. *Climatic Change,* **110,** 1005–1027, doi:10.1007/s10584-011-0101-1.

——, V. Kattsov, A. Barrett, M. Serreze, T. Pavlova, M. Holland, and W. N. Meier, 2012: Trends in Arctic sea ice extent from CMIP5, CMIP3 and observations. *Geophys. Res. Lett.,* **39,** L16502, doi:10.1029/2012GL052676.

Strong, C., G. Magnusdottir, and H. Stern, 2009: Observed feedback between winter sea ice and the North Atlantic Oscillation. *J. Climate,* **22,** 6021–6032.

Tang, Q., X. Zhang, X. Yang, and J. A. Francis, 2013: Cold winter extremes in northern continents linked to Arctic sea ice loss. *Environ. Res. Lett.,* **8,** 014036, doi:10.1088/1748-9326/8/1/014036.

Thompson, D. W. J., and J. M. Wallace, 2000: Annular modes in the extratropical circulation. Part I: Month-to-month variability. *J. Climate,* **13,** 1000–1016.